Chapter 1 Fundamentals on Adsorption, Membrane Filtration, and Advanced Oxidation Processes for Water Treatment

Robert Liang, Anming Hu, Mélisa Hatat-Fraile, and Norman Zhou

Abstract Water treatment is the processing of water to meet or achieve specified goals or standards set by regulatory agencies and end users. New water treatment technologies are being developed that need to be evaluated on a fundamental scientific and practical basis compared to traditional remediation processes. Recent advances in nanomaterial development for water treatment in the areas of filtration membranes, high surface area adsorbents, and efficient photocatalysts require approval for their effectiveness and safeness. Fundamental theories and concepts discussed in this chapter pertain to the areas of (i) adsorption and equilibrium isotherms (ii) pressure-driven membrane filtration and its rejection mechanisms for filtration and reverse osmosis processes; and (iii) advanced oxidation processes with a focus on semiconductor photocatalytic concepts.

1.1 Introduction

In the beginning of the twentieth century, many of the water treatment methods currently used today were already established [1]; these methods include mechanical separation, coagulation, chemical purification, disinfection, biological treatment,

R. Liang • M. Hatat-Fraile • N. Zhou

Department of Mechanical and Mechatronics Engineering, Centre for Advanced Materials Joining, University of Waterloo, 200 University Avenue West, Waterloo, ON N2L 3G1, Canada

Waterloo Institute for Nanotechnology, University of Waterloo, 200 University Avenue West, Waterloo, ON N2L 3G1, Canada

A. Hu (⊠)

Department of Mechanical, Aerospace and Biomedical Engineering, University of Tennessee, 414 Dougherty Engineering Building, Knoxville, TN 37996-2210, USA e-mail: ahu3@utk.edu

A. Hu and A. Apblett (eds.), *Nanotechnology for Water Treatment and Purification*, Lecture Notes in Nanoscale Science and Technology 22, DOI 10.1007/978-3-319-06578-6_1, © Springer International Publishing Switzerland 2014

1

aeration, and boiling. The conventional drinking water treatment process, consisting of coagulation, flocculation, sedimentation, filtration, and chlorine disinfection, was developed and optimized throughout the twentieth century as a robust system to remove contamination [2]. Additionally, several technologies were developed over this time to meet complex end user goals which include aeration to control taste and odor, ion exchange and reverse osmosis for inorganic species removal, and adsorption of organic species using activated carbon. Towards the end of the twentieth century, the most significant additions to water treatment were the development of membrane technologies and advanced oxidation processes (AOPs). Membrane technologies allow for the potential to completely remove particulates and pathogens via size exclusion on a scale as required by the end user. AOPs are capable of the oxidation of many pollutants into intermediate species and, eventually, their mineralization into inorganic compounds.

With the growing demand for clean water sources, there is rising concern regarding the availability and strategies necessary for the deliverance of potable water [3-6]. To exacerbate the situation, there are also emerging pollutants in wastewater effluents that have potential adverse health effects; these include, but are not limited to, textile dyes, pharmaceuticals and personal care products (PPCPs), endocrine disrupting compounds (EDCs), and plasticizers [3, 7–10]. The increasing network between receiving waters for treated wastewater and source water withdrawal has created the possibility of exposure to these trace contaminants through the water supply. Recent research has found evidence of low concentrations of PPCPs and EDCs in source waters in many developed communities, which have no regulations in place to control these contaminants [11]. PPCPs, including medical products, cosmetics, and pesticides, enter the wastewater system via human excreta or urine, washing, improper disposal, lawn care, etc. They have unknown side effects and consequences for human life and water ecosystems. Endocrine disrupting chemicals may disrupt the human endocrine system, which controls metabolic processes. Wastewater effluents are also high in nutrients and may cause algal blooms that release toxins into source water. Addressing current and future problems requires new robust methods and technologies of purifying water at lower cost, energy, and environmental impact than current methods.

Nanomaterials are materials that are modified or synthesized in the nanoscale (1–100 nm) using a bottom-up approach and can exhibit properties that are not observed in the macro or micro scale. They are promising solutions for water supplies contaminated by organic and inorganic compounds, heavy metal ions, and microorganisms [12]. Specifically, nanomaterials can improve on some existing treatment technologies including adsorption of contaminants, membrane filtration, and AOPs.

The focus of this chapter is to introduce the reader to the fundamental theories and concepts behind pollutant removal processes that use nanomaterials for water treatment, which are required to understand and evaluate nanomaterials against current benchmarks. The topics included in this chapter are the fundamentals of adsorption and the related adsorption equilibrium and isotherms; membrane filtration and reverse osmosis processes; and an overview of AOPs with a focus on photocatalytic degradation processes.

1.2 Adsorption

1.2.1 Introduction to Adsorption

Adsorption is the accumulation of substances at a surface interface through a mass transfer process. Lowitz, in 1785, first observed the phenomenon in solution and it was subsequently used in sugar refining processes for color removal [13]. The term itself was coined by Kayser (1881), but has been reported as early as 4000 BC in Sanskrit texts as a method to enhance the taste and odor of drinking water [14]. The mass transfer operation occurs when a substance, the adsorbate, present in the liquid phase diffuses and is accumulated and transferred onto a solid phase, the adsorbent. The reader is referred to several texts on adsorption, particularly on activated carbon, that underlie the concepts in this section [15–17].

1.2.2 Types of Adsorption

1.2.2.1 Chemical Adsorption

Chemical adsorption, also known as chemisorption, is a process that transpires when the adsorbate reacts with the adsorbent interface to form chemical or ionic bonds. The attractive forces of the adsorbent and adsorbate at the interface are akin to covalent bonds formed between atoms and obey Coulomb's law.

1.2.2.2 Physical Adsorption

Adsorbates undergo physical adsorption if the attractive forces are through physical forces that exclude covalent bonding with the interface and coulombic attraction. Physical adsorption and chemisorption are sometimes difficult to differentiate. Physical adsorption is reversible due to weaker forces and energies of bonding compared to chemisorption. Physical forces operate over longer distances than chemisorption and have no preferential surface adsorption sites.

In water treatment, the adsorption of organic molecules from water, a polar solvent, to a nonpolar adsorbent, such as activated carbon, is dictated by van der Waals forces that occur between organic substances and graphitic carbon planes in activated carbon. In general, increasingly larger and nonpolar compounds adsorb more intensely to nonpolar adsorbents due to hydrophobic bonding [18]. The attraction, due to van der Waals forces, at an adsorbate-activated carbon interface increases with increasing polarizability and size.

1.2.3 Adsorption Materials

The most common commercial adsorbent used in water remediation is activated carbon, but there are others worth mentioning, such as zeolites and synthetic polymers. In order to classify the pore sizes of these adsorbents, the IUPAC defines pore classifications into three classes: macropores (>25 nm), mesopores (1–25 nm), and micropores (<1 nm). Zeolites (aluminosilicates) have very small pore sizes, which are capable of excluding some organic compounds. Synthetic polymer adsorbents usually have micropore distributions, which prevent them from adsorbing natural organic matter (NOM). Activated carbon has a range of pore sizes, depending on the manufacturing process, and can adsorb large organic molecules such as NOM and synthetic organic compounds (solvents, fuels, pesticides, and others). In addition to the commercial adsorbents, research has also been conducted on nanomaterials such as carbon nanotubes [19] and graphene [20] due to their high sorption capacity. Non-conventional low-cost adsorbents are continuously being sought after in order to improve performance to cost ratios [21].

1.2.3.1 Activated Carbon

Activated carbon is typically made from organic materials (coconut husks, wood, peat, coal, and synthetic sources) that are heated to high temperatures (>700 °C) and pyrolized in an oxygen-deprived environment. In water treatment, it is used in either of two forms: granular-activated carbon (GAC) and powder-activated carbon (PAC). PAC (mean particle size: $20-50~\mu m$) is usually added directly to water sources at various stages of the water treatment process and is removed through sedimentation or filtration. GAC (mean particle size: 0.5-3~mm) is typically employed as a fixed bed after filtration and before disinfection. GAC can also be impregnated with iron to remove arsenic, ammonia to increase adsorption capacity for anionic species, and silver for disinfection properties [22].

1.2.3.2 Non-conventional Low-Cost Adsorbents

There is a need for non-conventional low-cost adsorbents because the thermal input required to manufacture activated carbon makes it relatively expensive. These low-cost adsorbents should be effective, but also abundant in nature, inexpensive, and require minimal processing. A list of non-conventional adsorbents is given in Table 1.1. These adsorbents are usually made from agriculture and industry by-products, natural materials, and biosorbents that contain high surface area and porosity [23].

Adsorbent Example References Agriculture and industry waste Teak wood bark **[24]** Papava seeds [25] Sugar industry mud [26] Grass waste [27] [28, 29] Peels (pomelo, jackfruit, banana, garlic) Rubber seed shell [30] Fly ash [31, 32]Coconut tree flower [33] Natural materials Clay (montmorillonite, bentonite, [34–38] fibrous clay, palygorskite, kaolin) Glass wool [39] Bioadsorbents Biomass (algae, activated sludge) [40-46] Fungi [47, 48]Microbial [49]

Table 1.1 List of nonconventional adsorbents

Adapted from Crittenden et al. (2012), Ref. [22]

1.2.4 Important Factors Involved in Adsorption

1.2.4.1 Surface Area and Pore size

Surface area and pore size are important factors that determine the number and availability of adsorption sites for adsorbates. Typically, there is an inverse relationship between surface area and pore size; in other words, the smaller the pore size of a given volume of absorbent, the greater the surface area that is available for the adsorption process. Additionally, depending on the size of the adsorbate and adsorbent pores, adsorption may be limited by steric effects. Adsorbents with large porosities are brittle and tend to break apart.

1.2.4.2 Background Matrix Effects

One factor that affects adsorption efficiency of a target compound is the influence of the water matrix. Increases in the concentrations of naturally occurring or anthropogenic compounds in the background matrix will decrease the adsorption capacity of the target compound due to competitive adsorption onto the adsorption sites.

1.2.5 Adsorption Kinetics

The removal of a compound by adsorbents is a three-step process: external mass transfer (EMT), internal mass transfer (IMT), and adsorption (Fig. 1.1). Both EMT and IMT are considered to be diffusion-based processes and the driving force is the

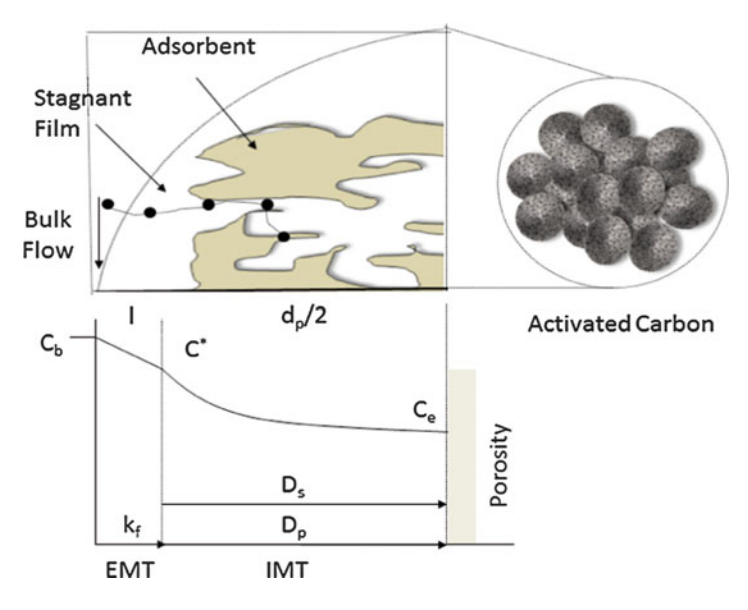


Fig. 1.1 Illustration of mass transfer and adsorption processes, Ref. [17]

concentration gradient of the adsorbate; the difference between the bulk concentration ($C_{\rm b}$) and the internal concentration at equilibrium ($C_{\rm e}$). In the first step, EMT, or film diffusion, of the compound from the bulk liquid phase occurs through the hydrodynamic layer that surrounds the adsorbent. After EMT occurs and delivers the adsorbate to the external surface of the adsorbent, IMT delivers the compound to an adsorption site. IMT occurs either through the pore fluid or pore wall through pore diffusion ($D_{\rm p}$) and surface diffusion ($D_{\rm s}$). These diffusional processes are controlled by the pore structure or adsorbate properties. The IMT is often the slowest and thus controls the overall uptake of an adsorbate. The actual adsorption of the adsorbate, the final step, occurs quickly and is not considered rate-limiting.

1.2.6 Adsorption Equilibrium

Adsorption isotherms are used to quantify the quantity of adsorbate that an adsorbent can adsorb at equilibrium conditions and constant temperature. From an experiment that varies the adsorbent dose and/or the initial adsorbate concentration, the equilibrium solid-phase adsorbate concentration can be calculated, and a relationship with the equilibrium liquid-phase concentration can be established.

This adsorption equilibrium relationship is termed the isotherm and allows the adsorption capacity of the adsorbent to be calculated at any given liquid-phase adsorbate concentration. The equilibrium capacity is calculated using a mass balance expression [22]:

$$q_e = \frac{V}{M}(C_o - C_e) \tag{1.1}$$

where q_e is equilibrium concentration of adsorbate (mg g⁻¹), C_o is initial concentration of adsorbate (mg L⁻¹), C_e is equilibrium concentration of adsorbate (mg L⁻¹), V is volume of aqueous solution added to bottle (L), and M is mass of adsorbent (g).

Some isotherms commonly used in research are the Langmuir, Brauener-Emmett-Teller (BET), Freundlich, and Redlich-Peterson isotherms.

1.2.6.1 Langmuir Isotherm

The Langmuir adsorption isotherm describes the reversible chemical equilibrium between species at the surface-solution interface [50]. The chemical reaction defines adsorbate species (A), which diffuses to vacant surface sites (S_v) , to form adsorbate species bound to surface sites (SA):

$$S_{\rm v} + A \leftrightarrow SA$$
 (1.2)

where S_v is vacant surface sites (mmol m⁻²), A is adsorbate species in solution, (mmol), and SA is adsorbate species bound to surface sites (mmol m⁻²).

In Eq. (1.1), the reaction is assumed to have a constant value for free energy change ($\Delta G_{\rm ads}^o$) for all surface sites. Each site is capable of binding only one molecule or, in other words, the model only allows for accumulation of adsorbates up to a monolayer on the adsorbent. The equilibrium equation is written as:

$$K_{\rm ad} = \frac{SA}{S_{\rm v}C_A} = {\rm e}^{-\Delta G_{\rm ads}^o/RT}$$
 (1.3)

where $K_{\rm ad}$ is adsorption adsorbent-phase equilibrium constant (L mg⁻¹), C_A is equilibrium adsorbent-phase concentration of adsorbate A in solution (mg L⁻¹), $\Delta G_{\rm ads}^o$ is free-energy change for adsorption (J mol⁻¹), R is universal gas constant, 8.314 J K⁻¹ mol⁻¹, and T is absolute temperature (K).

Equation (1.3) can be expressed much more conveniently by fixing the total number sites and eliminating $S_{\rm V}$ as an unknown:

$$S_T = S_V + SA = \frac{SA}{K_{ad}C_A} + SA \tag{1.4}$$

where S_T is total number of sites available or monolayer coverage.

Rearranging Eq. (1.4) for SA gives:

$$SA = \frac{S_T}{1 + \frac{1}{K_{vd}C_A}} = \frac{K_{ad}C_AS_T}{1 + K_{ad}C_A}$$
 (1.5)

Equation (1.5) can be expressed in terms of mass loading, q_A :

$$q_A = (SA)(A_{ad})(MW) = \frac{K_{ad}C_AS_TA_{ad}MW}{1 + K_{ad}C_A} = \frac{Q_MK_{ad}C_A}{1 + K_{ad}C_A} = \frac{Q_Mb_AC_A}{1 + b_AC_A}$$
(1.6)

where q_A is equilibrium adsorbent-phase concentration of adsorbate A, (mg adsorbate g^{-1}) adsorbent, A_{ad} is surface area per gram of adsorbent (m² g⁻¹), MW is molecular weight of adsorbate A (g mol⁻¹), C_A is equilibrium adsorbent-phase concentration of adsorbate A in solution (mg L⁻¹), Q_M is maximum adsorbent-phase concentration of adsorbate A when surface sites are saturated with adsorbate, (mg adsorbate g⁻¹ adsorbent), b_A is Langmuir adsorption constant of adsorbate A, K_{ad} , (L mg⁻¹).

It is also convenient to rearrange Eq. (1.6) to a linear form:

$$\frac{C_A}{q_A} = \frac{1}{b_A Q_M} + \frac{C_A}{Q_M} \tag{1.7}$$

A plot of C_A/q_A versus C_A results in a straight line with slope of $1/Q_M$ and intercept $1/b_AQ_M$.

1.2.6.2 Brunauer–Emmett–Teller Adsorption Isotherm

The BET adsorption isotherm [51] is an extension of the Langmuir model. Specifically, in order to accommodate multilayer adsorption at greater pressures, the BET isotherm expands on the assumption that a monolayer of molecules is formed during adsorption. Each additional layer of adsorbate molecules is in equilibrium with subsequent layers below it, which can vary in thickness. A consequence of the BET model is that it will always generate a smaller value for the predicted surface area compared to the Langmuir isotherm due to potential adsorbate layering of the material. The equation is:

$$\frac{q_A}{Q_M} = \frac{B_A C_A}{\left(C_{S,A} - C_A\right) \left[1 + \left(B_A - 1\right) \left(\frac{C_A}{C_{S,A}}\right)\right]} \tag{1.8}$$

$$B_A = \frac{K_{1,\text{ad}}}{K_{i,\text{ad}}} = \frac{e^{-\Delta G_{\text{ads}}^o}}{e^{-\Delta G_{\text{prec}}^o}}$$
(1.9)

where q_A is equilibrium adsorbent-phase concentration of adsorbate A (mg g⁻¹), Q_M is maximum adsorbent-phase concentration of adsorbate when surface sites are saturated with adsorbate (mg g⁻¹), $K_{1,ad}$ is equilibrium constant for first layer

(L mg⁻¹), $K_{i,ad}$ is equilibrium constant for lower layers (L mg⁻¹), B_A is ratio of $K_{1,ad}$ and $K_{i,ad}$, C_A is equilibrium concentration of adsorbate A in solution (mg L⁻¹), $C_{S,A}$ is saturated solution concentration of A (mg L⁻¹), ΔG_{ads}^o is free energy of adsorption (J mol⁻¹), and ΔG_{prec}^o is free energy of precipitation (J mol⁻¹).

In the Langmuir model, the site energy for adsorption is equal for all surface sites and the largest capacity is one monolayer. These assumptions are not valid for many adsorbents, such as activated carbon. Although the BET isotherm allows for many layers to be modeled, it is assumed in Eq. (1.8) that site energy is equal to the first layer and to the free energy of precipitation for additional lower layers. In actuality, the site energy of adsorption is variable for most adsorbents because they are quite heterogeneous in nature. Often, in the cases of heterogeneous adsorbents with varying site energies, the Freundlich equation is used to describe isotherm data.

1.2.6.3 Freundlich Isotherm

The Freundlich adsorption isotherm [52] equation can be used to model data for heterogeneous adsorbents and is a better fit for GAC isotherm data than the Langmuir equation [53]. The equation is:

$$q_a = K_A C_A^{\frac{1}{n}} \tag{1.10}$$

where K_A is Freundlich adsorption capacity parameter, $(mg/g) (L/mg)^{1/n}$ and 1/n is Freundlich adsorption intensity parameter, unitless.

The Freundlich equation (Eq. (1.10)) is derived from the Langmuir equation (Eq. (1.5)) to model the adsorption of adsorbates onto surface sites of a given free energy with two additional assumptions: (i) the surface site energies for adsorption tend to a Boltzmann distribution with mean site energy ΔH_M^o and (ii) the change in surface site entropy is a linear function of site enthalpy $-\Delta H_{\rm ad}^o$. Given these assumptions, the Freundlich adsorption intensity parameter, n^{-1} , is:

$$n = \frac{\Delta H_M^o}{RT} - \frac{r\Delta H_{\text{ad}}^o}{R} \tag{1.11}$$

where ΔH_M^o is mean site energy (J mol⁻¹), R is universal gas constant, 8.314 J K⁻¹ mol⁻¹, $\Delta H_{\rm ad}^o$ is change in site enthalpy (J mol⁻¹), T is absolute temperature (K), and r is proportionality constant.

1.2.6.4 Redlich-Peterson Isotherm

The Redlich-Peterson isotherm [54] combines features from the Langmuir and Freundlich equation. It is designated as a three parameter equation used to represent adsorption equilibria over a wider concentration range:

$$q_{A} = \frac{K_{R-P}C_{A}}{1 + \alpha_{R-P}C_{A}^{\beta}} \tag{1.12}$$

where K_{R-P} is Redlich-Peterson parameter (L mg⁻¹), α_{R-P} is Redlich-Peterson parameter (L mg⁻¹), and β is heterogeneity factor (values between 0 and 1).

Equation (1.12) approaches the Langmuir equation when β approaches 1, and become's Henry's law equation when $\beta = 0$.

1.3 Membrane Filtration and Reverse Osmosis

1.3.1 Introduction

A membrane is a physical interface which separates two phases, forming a barrier to the transport of matter. Membranes have microscopic openings that allow water molecules to pass, but not compounds that are larger than the opening. Membrane filtration can be operated either as dead-end filtration or cross-flow filtration as shown in Fig. 1.2. In dead end filtration, the feed water flows perpendicular to the membrane surface; all solids will amass onto the membrane surface during filtration and are removed via backwashing. The accumulation of solids in dead-end filtration often results in a lower flux compared to cross-flow filtration.

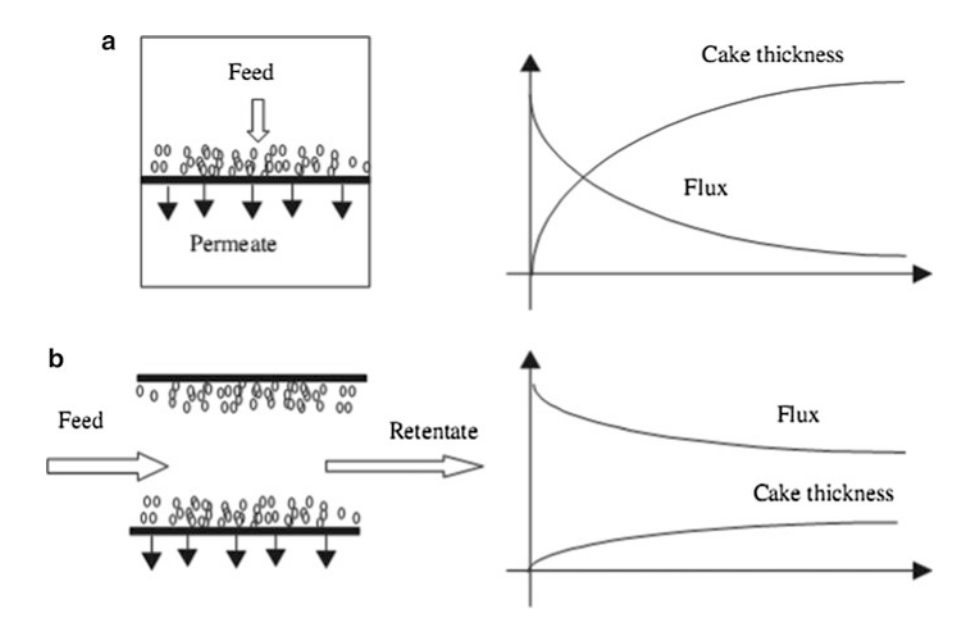


Fig. 1.2 Schematic of (a) dead-end and (b) cross-flow filtration (Source: Li (2007), Ref. [56])

In cross-flow filtration, the feed water is parallel to the membrane surface. The flow velocity parallel to the surface of the membrane generates a shear force that reduces the growth of a filter cake [55]. Since the majority of solids pass with the retentate instead of collecting on the membrane surface, the system can function at higher flux.

1.3.2 Membrane Materials, Properties, and Geometries

1.3.2.1 Membrane Materials

Most membranes are made from synthetic organic polymers, which can be either hydrophobic or hydrophilic. Hydrophilic polymer membranes include cellulose and its derivatives, polyacrylonitrile, hydrophilized polysulfone, hydrophilized polyethylene, and others. Hydrophobic membranes include polytetrafluroethylene (PTFE), polyethylene (PE), polyvinylidene fluoride (PVDF), and many more.

Additionally, membranes can be prepared from inorganic materials, including metals and ceramics. Inorganic membranes are used because of their high stability at high temperatures (over 100 °C) and at extreme pH, but are brittle due to their crystal structure. Ceramic materials, for the most part, are composite materials consisting of one or many different ceramic materials. They have a macroporous support, followed by a few layers of microporous top layers. The most commonly used materials for ceramic membranes are alumina (Al₂O₃), titanium dioxide (TiO₂), zirconium dioxide (ZrO₂), silicon dioxide (SiO₂), or a mixture of these materials.

1.3.2.2 Membrane Properties

Membranes have pore sizes ranging from $0.5 \, \mathrm{nm}$ to $5 \, \mu \mathrm{m}$, which may be determined by bubble point analysis, microscopic analysis, or porosimetry. Membrane manufacturers also use the molecular weight cutoff (MWCO) to characterize the apparent size of particles that are retained. It is a parameter defined as the lower limit of a molecular weight of a solute for which the rejection is 95–98 %. The MWCO is an indicator of the membrane's actual ability to remove a given compound because factors other than membrane pore size (polarity, molecular shape, and surface interaction with the membrane) affect rejection characteristics [57].

Testing properties other than pore size are often necessary. Surface properties such as surface roughness, charge, hydrophobicity, and chemistry are necessary in determining the effectiveness of the membrane. From a commercial standpoint, a performance over cost ratio in terms of durability, stability, and effectiveness of membranes is necessary. Table 1.2 lists some of the properties that can be analyzed and the impact of each property on the performance of the membrane.

 Table 1.2 Important properties of membranes and their method of determination and impact on performance

Property	Method of determination	Impact on membrane performance
Surface roughness	Atomic force microscopy	Rough materials will tend to foul more than smooth materials
Surface charge	Streaming potential	Repulsive forces between a charged membrane and ionic species can reduce fouling by minimizing contact between the membrane and foulant
Hydrophobicity	Contact angle	Hydrophobic materials are, generally, more prone to fouling than hydrophilic materials
Surface chemistry	ATR-FTIR, SIMS, XPS	The surface composition affects cleaning and fouling by influencing interactions between the membrane surfaces and constituents in the feed solution
Porosity	Thickness/weight measurements	Affects the head loss through a given membrane; higher porosity of the membrane will result in lower head loss
Mechanical durability	Mechanical tests	Affects the ability of the material to withstand stressors in the form of surges due to imperfect operation of mechanical pumps and valves
Cost	Material cost	Affects the cost of the membrane system
Chlorine/oxidant tolerance		Affects the ability to disinfect the membrane equipment after use. Increasing the tolerance of the membrane to these chemicals increases the longevity of the membrane
Biological stability	Exposure to organisms	Affects the life span of the membrane; low biological stability can result in microorganism colonization and the degradation of the membrane by these microorganisms
Chemical and thermal stability	Exposure to chemical, pH, and temperature extremes	Affects the life span of the membrane; greater chemical and temperature tolerance allows for harsher, but more effective cleaning procedures with less degradation of the material

Adapted from Crittenden et al. (2012), Ref. [22]

1.3.2.3 Membrane Configurations

Membranes are fabricated into four configurations: (i) flat sheet and plate and frame, (ii) hollow fiber, (iii) tubular, and (iv) spiral wound. The flat sheet and plate and frame configuration is commonly used for laboratory separations. Hollow fiber and spiral wound membrane configurations are often used for NF and RO membranes. The tubular configuration is preferred for ceramic membranes that have low packing densities. These configurations are illustrated and described in Table 1.3.

Configuration Schematic Description Permeate Flat sheet and Membranes are flat sheets and plate and used as a laver or several frame layers interspersed with a Retentate frame in a filtration cell. They are common in laboratory eed Spacer separations, but difficult to Mesh implement at a large scale Permeate Potting Hollow Membranes are made as hollow Hollow Material fiber and tubes. They are the most Fibers Pressure hollowcommon configuration in Vessel Cell membrane filtration for fine fiber Retentate water treatment Permeate Tubular Ceramic Membranes are made into Support Ceramic monoliths with channels Membrane through the structure. Tubular membranes are often constructed using ceramic membranes, which have low packing densities but can Retentate operate at high cross-flow Permeate velocity, where solute concentration is very high Spiral wound These are many flat sheet membranes that are stacked Retentate and bundled around the center of a tube so that the permeate will travel via a spiral flow path toward the collection tube at the center. These are used often in NF and RO membranes, but not used in membrane filtration due to clogging of large particulates and backwashing problems

Table 1.3 Description and schematic of various membrane configurations

1.3.3 Membrane Processes

There are four distinguishable types of pressure-driven membrane processes: microfiltration (MF), ultrafiltration (UF), nanofiltration (NF), and reverse osmosis (RO). These membrane processes can also be separated into two classes: (i) membrane filtration (microfiltration and ultrafiltration) and (ii) reverse osmosis (and nanofiltration). Microfiltration and ultrafiltration are governed by Darcy's law, whereas nanofiltration and reverse osmosis are governed by Fick's law. These pressured-driven processes are illustrated in Table 1.4.

14

Table 1.4 Pressure-driven membrane processes

	•			
Process	Separation concept	Pressure required (atm)	Materials passed	Governing equations
Microfiltration	Feed ———————————————————————————————————	1–5	Water and dissolved species	Darcy's law
Ultrafiltration	Feed — Concentrate	2–10	Water and salts	Darcy's law
Nanofiltration Reverse Osmosis	Saline water feed Semi-permeable membrane	5-50 10-100	Water and monovalent ions Water	Fick's law

Mechanism for rejection Diagram Description Particles larger than the pores are Sieving Particle retained Membrane Adsorption Colloidal matter adsorbed Adsorption occurs when particulates to wall of pores are small enough to adsorb to the walls of pores Cake formation Smaller particles Small particles are unable to pass trapped by cake layer through the membrane and are retained due to the accumulation Cake layer of larger materials that amass at the membrane surface

Table 1.5 Description of sieving, adsorption, and cake formation processes

Adapted from Crittenden et al. (2012), Ref. [22]

MF membranes have large pore sizes and reject large particulates and microorganisms. UF membranes have smaller pores than MF membranes and can reject bacteria and soluble macromolecules. RO membranes are, for the most part, nonporous and reject particulates and numerous low molecular weight species such as salt ions and small organics molecules. NF membranes are thought of as a "loose" RO membrane exhibiting performance parameters between UF and RO membranes.

1.3.3.1 Microfiltration and Ultrafiltration

Filtration in microfiltration and ultrafiltration is governed by Darcy's law and proceeds in three steps: (i) sieving, (ii) adsorption, (iii) and cake formation. Illustrated in Table 1.5, these mechanisms are critical in understanding and evaluating performance. Sieving, or straining, is the primary filtration mechanism in which particles larger than the MWCO collect at the surface of the membrane, while smaller particles in the water pass through. However, as mentioned before, particulate removal is not an ideal step function at the MWCO because of the properties of the membrane and particle-membrane interface interactions.

NOM is capable of adsorbing to membrane surfaces. Soluble substances may be excluded despite their physical dimensions being smaller than the MWCO. Adsorption plays a role in the primary stage of filtration using a clean membrane; however, the adsorption capacity is eventually exhausted and is not an effective mechanism for long-term filter use. Adsorption can have a significant impact on the operation of the membrane. Adsorbed material can decrease the MWCO by decreasing the size of pore cavities throughout the membrane, thus increasing the capability to retain smaller material via sieving. Furthermore, due to decreasing the MWCO, adsorption of NOM causes membrane fouling.

During filtration, a clean membrane will accumulate particles at the surface due to the sieving process. The accumulation of solids forms a particulate cake, which acts as a filtration medium that is dynamic in that its capability varies as a function of time from cake growth and backwashing processes.

The flow of feed water through MF and UF membranes follows Darcy's law for superficial fluid velocity:

$$v = \frac{k_P h_L}{L} \tag{1.13}$$

where k_P is hydraulic permeability coefficient (m s⁻¹), h_L is head loss across porous medium (m), and L is thickness of porous medium (m).

The hydraulic permeability coefficient, k_P , in Eq. (1.13) is empirically obtained and is dependent on porosity and surface area of the membrane. The membrane flux equation incorporates the membrane thickness and the resistance coefficient; it is stated as:

$$J = \frac{Q}{a} = \frac{\Delta P}{\mu \kappa_m} \tag{1.14}$$

where J is water flux through membrane (L m⁻² s⁻¹), Q is flow rate (L s⁻¹), a is membrane area (m²), ΔP is differential pressure across membrane (bar), μ is dynamic viscosity of water (kg m⁻¹ s⁻¹), and κ_m is membrane resistance coefficient (m⁻¹).

1.3.3.2 Nanofiltration and Reverse Osmosis

Osmosis is a process of flow through a semipermeable membrane. Under isothermal ($\Delta T = 0$) and isobaric ($\Delta P = 0$) conditions between the two sides of the membrane, no water will flow through the membrane. However, when solutes are dissolved into the water on one side, a flow through the membrane from the pure water to the water containing salts will occur. In other words, the concentration of solutes will tend toward being equal on both sides.

Reverse osmosis is the process where pressure is applied on the side of the membrane where salts are added. The extra pressure will result in a flow of water through the membrane, but the salts do not flow through because of the membrane pore size.

In other words, reverse osmosis exploits two opposing forces: (i) the concentration gradient and (ii) the pressure gradient. Reverse osmosis is always operated under cross-flow conditions. The rejection of solutes of a RO and NF membranes is defined by salt rejection, given by:

$$Rej = 1 - \frac{C_P}{C_F} \tag{1.15}$$

Rej is rejection (dimensionless), C_P is concentration of permeate (mol L⁻¹), and C_E is concentration in feed water (mol L⁻¹).

Equation (1.15) can be calculated from parameters such as total dissolved solids (TDS) or conductivity. Sodium chloride (NaCl) rejection is used as the standard for high pressure RO membranes, whereas magnesium sulfate (MgSO₄) is used as the standard for NF and low pressure RO membranes.

1.3.3.2.1 Kinetic Equations

Flux

The flux, J, is the permeate flow through one square meter of membrane surface:

$$J = \frac{\Delta P_{\text{trans}}}{\mu \kappa_m} \tag{1.16}$$

where ΔP_{trans} is transmembrane pressure (Pa), μ is dynamic viscosity of water (N s m⁻²), κ_m is membrane resistance coefficient (m⁻¹), and C_F is concentration in feed water (mol L⁻¹).

From Eq. (1.16), the net transmembrane pressure, $\Delta P_{\text{trans}_{\text{net}}}$, is a driving force for RO and NF membranes and is given by:

$$\Delta P_{\text{trans}_{\text{net}}} = \Delta P - \Delta \Pi = P_f - \frac{\Delta P_{\text{hyd}}}{2} - P_p - \Delta \Pi$$

$$\Delta P_{\text{hyd}} = P_f - P_c$$
(1.17)

where P_f is pressure of feed (Pa), $\Delta P_{\rm hyd}$ is hydraulic pressure loss (Pa), P_p is pressure of permeate (Pa), $\Delta \Pi$ is osmostic pressure difference (Pa), and P_c is pressure of concentrate (Pa).

Osmotic Pressure

The reverse osmosis (including nanofiltration) driving force for diffusion is via a concentration gradient, or in thermodynamic terms, a gradient in Gibbs energy [58]. To describe osmosis, the general form of the Gibbs function is used:

$$\delta G = V \, \delta P - S \, \delta T + \Sigma_i \mu_i^{\,o} \delta n_i \tag{1.18}$$

G is Gibbs energy (J), *V* is volume (m³), *P* is pressure (Pa), *S* is entropy (J K⁻¹), *T* is absolute temperature (K), μ_i^o is chemical potential of solute I (J mol⁻¹), and n_i is amount of solute I in solution (mol).

The chemical potential is defined as:

$$\mu_i^o = \frac{\delta G}{\delta n_i} \bigg|_{P,T} \tag{1.19}$$

The last term in Eq. (1.18) describes the difference in Gibbs energy between the amount of solute in the feed and permeate sides. When volume is constant, the difference in the amount of solute equals the difference in concentrations. Under constant temperature ($\delta T = 0$), equilibrium occurs when the summation of the Gibbs energy gradient due to the chemical potential is counterbalanced by the pressure gradient between the feed and permeate sides:

$$V\delta P = -\Sigma_i \mu_i^o \delta n_i \quad \text{when } \delta G = 0 \tag{1.20}$$

To balance the difference in chemical potential of a solute, the pressure required is known as the osmotic pressure and denoted as Π . When the vessel reaches equilibrium conditions, the difference in hydrostatic pressure is equal to the difference in osmotic pressure between the two sides. The osmotic pressure can be derived using a thermodynamic treatment with the assumptions that the solution is incompressible and behaves ideally:

$$\Pi = -\frac{RT}{V_b} \ln(x_w) \tag{1.21}$$

where Π is osmotic pressure (bar), V_b is molar volume of pure water (L mol⁻¹), x_w is mole fraction of water (mol mol⁻¹), T is temperature (K), and R is universal gas constant, 0.083145 (L bar K⁻¹ mol⁻¹).

In dilute solution (i.e., $x_w = 1$), Eq. (1.21) can be approximated by the van't Hoff equation for osmotic pressure, which has the same form as the ideal gas law (PV = nRT):

$$\Pi = \frac{n_S}{V}RT = CRT \tag{1.22}$$

where Π is osmotic pressure (bar), n_s is total amount of all solutes in solution (mol), C is concentration of all solutes (mol L⁻¹), and V is volume of solution (L).

To account for the assumption of diluteness, the nonideal behavior of concentrated solutions, and the compressibility of liquid at high pressure, a nonideality coefficient (osmotic coefficient ϕ) must be incorporated into Eq. (1.22):

$$\Pi = \phi \text{ CRT} \tag{1.23}$$

where ϕ is osmotic coefficient (unitless).

Osmotic Pressure Difference

The osmotic pressure difference over a membrane, $\Delta\Pi$, is given by:

$$\Delta\Pi = \frac{\Pi_f + \Pi_c}{2} - \Pi_p \tag{1.24}$$

where Π_f is osmotic pressure of feed (Pa), Π_c is osmotic pressure of concentrate (Pa), and Π_p is concentration of permeate (Pa).

Because the concentration of salts in the permeate feed is very low, the osmotic pressure in the permeate feed is almost always neglected. On the other hand, the osmotic pressure of the concentrate, Π_c , is higher than the osmotic pressure of the feed, Π_f . The osmotic pressure of the concentrate can be put in terms of the osmotic pressure of the feed:

$$\Pi_{\rm c} = \Pi_{\rm f} \left(\frac{1}{1 - \gamma} \right) \tag{1.25}$$

$$\gamma = \frac{Q_p}{Q_f} \tag{1.26}$$

 γ is recovery, Q_p is permeate flow (m³ h⁻¹), and Q_f is feed flow (m³ h⁻¹).

Combining Eq. (1.24) with Eq. (1.25), the osmotic pressure difference over a membrane can be written as:

$$\Delta\Pi = \Pi_f \frac{2 - \gamma}{2(1 - \gamma)} \tag{1.27}$$

1.3.3.2.2 Concentration Polarization

Concentration polarization is the accumulation of solutes close to the proximity of the surface of the membrane causing a decrease in performance. The exclusion mechanisms for solutes differ from particles because solutes stay in solution and form a concentration gradient with the highest concentration near the boundary layer of the adsorbent and liquid phase, causing polarization. The resulting effects due to concentration polarization are that: (i) water flux is lower due to higher osmotic pressure, (ii) rejection is lower due to the increase in concentration at the membrane and decrease in flux, and (iii) solubility limits of solute at or near the membrane may be exceeded and cause fouling, specifically precipitation or scaling (Fig. 1.3a).

Concentration polarization is reversible and will disappear as the driving force tends to zero. Concentration polarization can be limited with disturbance to the boundary layer via increasing the velocity along the membrane surface. The relationship between concentration close to the membrane surface and in the feed (Fig. 1.3b) is represented by the concentration polarization factor (β) , which is given by:

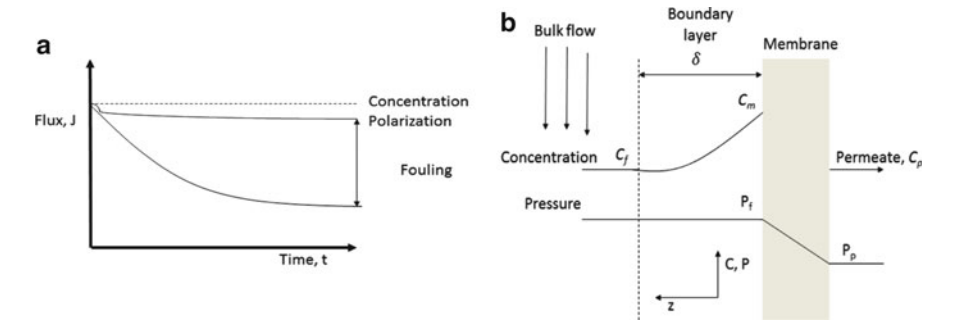


Fig. 1.3 (a) Concentration polarization and fouling during cross-flow operation and (b) schematic of concentration polarization near the membrane

$$\beta = \frac{C_m - C_p}{C_f - C_p} = e^{\frac{I\delta}{D}} \tag{1.28}$$

where C_p is concentration in permeate (mol L⁻¹), C_m is concentration in membrane (mol L⁻¹), C_f is concentration in feed (mol L⁻¹), J is permeate flux (ms⁻¹), δ is thickness of boundary layer (m), and D is diffusion coefficient (m²s⁻¹).

 C_p can be neglected because $C_p \ll C_f < C_m$ and the coefficient k is taken for the mass transfer and the following relation can be used:

$$k = \frac{D}{\delta} \tag{1.29}$$

 β can be rewritten as:

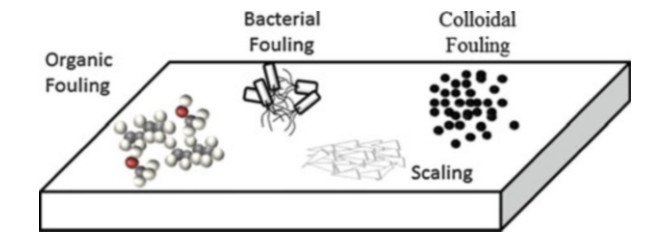
$$\beta = \frac{C_m}{C_f} = e^{\frac{J}{k}} \tag{1.30}$$

The high concentration polarization given by the factor β leads to higher osmotic pressure difference across the membrane and therefore lowers the performance of the membrane.

1.3.4 Membrane Fouling

A major problem of membranes is fouling. Fouling occurs on the surface of the membrane and/or within the pores of the membrane and is detrimental in that it reduces flux. The types of fouling are shown in Fig. 1.4, which include biofouling, organic, colloidal, and scaling. Biofouling results from microorgranism contamination of the feed water and produces a biofilm on the surface of the membranes. Organic fouling comes from substances such as hydrocarbons, dyes, and pesticides, which coat the surface and/or plug pores. Colloidal fouling mainly stems from

Fig. 1.4 Fouling of membranes under organic, bacterial, colloidal, and precipitate (scaling) contaminants



particles, such as silica and clay, collecting on the surface of the membrane. Scaling arises from the deposition and precipitation of salts onto the membrane.

1.3.4.1 Biofouling

Biofouling is defined as the loss of system performance due to the formation of a biofilm; a layer of microorganisms attached to the membrane surface [59]. The microorganisms can attach to the membrane quite strongly so that backwashing removal steps prove insufficient. To exacerbate the problem, they also produce extracellular material that can act as foulants. These biofoulants can typically be addressed using chlorine disinfectants in the feed water and/or backwashing.

1.3.4.2 Organic Fouling

The most problematic membrane fouling is due to the adsorption of NOM at the membrane surface. The ability of dissolved organic matter (DOM) to adsorb to membranes has been demonstrated, with humic and fulvic solutions [60, 61]. Studies have also shown removing even a large fraction of DOM has little or no reduction of fouling [62, 63] and removing a small fraction of DOM can completely eliminate fouling [64]. Collectively, this research indicates that membrane fouling can be modeled by a power law. In other words, only a fraction of DOM causes the majority of fouling in membrane filtration, and high molecular weight and colloidal fractions cause the constriction of the membrane pores.

1.3.4.3 Precipitation and Scaling

Precipitation of ions is an import factor that limits recovery in RO systems. To limit precipitation, the salt rejection rate, the recovery, and the degree of concentration polarization is important because precipitation occurs in close proximity to the membrane surface. Concentration polarization is reduced by achieving turbulence and maintaining minimum velocity in feed channels. The most common scales encountered are calcium carbonate (CaCO₃) and calcium sulfate (CaSO₄), but there are other scales that occur as well, as shown in Table 1.6. Pretreatment

Salt	Equilibrium equation	Solubility of product (pK _{sp} , 25 °C)
Calcium carbonate	$CaCO_3(s) \leftrightarrow Ca^{2+} + CO_3^{2-}$	8.2
Calcium fluoride	$CaF_2(s) \leftrightarrow Ca^{2+} + 2 F^-$	10.3
Calcium orthophosphate	$CaHPO_4(s) \leftrightarrow Ca^{2+} + HPO_4^{2-}$	6.6
Calcium sulfate	$CaSO_4(s) \leftrightarrow Ca^{2+} + SO_4^{2-}$	4.6
Strontium sulfate	$SrSO_4(s) \leftrightarrow Sr^{2+} + SO_4^{2-}$	6.2
Barium sulfate	$BaSO_4(s) \leftrightarrow Ba^{2+} + SO_4^{2-}$	9.7
Silica, amorphous	$SiO_2(s) + 2H_2O \leftrightarrow Si(OH)_4(aq)$	2.7

Table 1.6 Common salts, their solubility, and dissociated ions

Source: Stumm and Morgan (1996), Ref. [65]

steps such as acidic pH adjustment of calcium carbonate can be used to produce bicarbonate and carbon dioxide and prevent precipitation. Additionally, antiscalent chemicals can be used to allow for supersaturation without precipitation by preventing crystal growth.

1.4 AOPs and Photocatalysis

1.4.1 Introduction

The goal of advanced oxidation processes (AOPs) is to oxidize organic pollutants in water via hydroxyl radicals (HO') thereby converting the constituents of the organic pollutants into relatively harmless organic or inorganic molecules. HO' radicals are very powerful oxidants that are highly reactive, non-selective electrophilic oxidizing agents, and are ubiquitous in nature [9]. In addition, HO' radicals react 10^6-10^{12} times more rapidly than alternative oxidants such as ozone (O₃) and have a high redox potential (2.80 V vs. normal hydrogen electrode, NHE) second only to fluorine, which is highly toxic [9, 66, 67]. A list of common oxidants is shown in Table 1.7.

1.4.2 Overview of AOP Processes

AOPs can be subdivided into the following processes: photo-induced processes, ozonation, Fenton process, photo-Fenton process, photosensitized process, and ultrasound. These processes generate hydroxyl radicals coming from chemical, photochemical, and sonochemical methods. A description of the processes and their reaction mechanism, shown in Table 1.8, and their advantages and disadvantages, shown in Table 1.9, are covered.

Table 1.7 Redox potentials of common oxidants

Oxidant	Redox potential (V vs NHE, 25 °C)
$\overline{F_2}$	+3.03
HO^{\bullet}	+2.80
O^{\bullet}	+2.42
O_3	+2.07
H_2O_2	+1.78
HO_2^{\bullet}	+1.70
Cl_2	+1.36

Source: Belgiorno et al. (2011), Ref. [9]

1.4.2.1 Photo-Induced Processes

Photo-induced processes can be thought of as either a photolysis process or a photochemical process. Photolysis is the use of radiant energy from UV-A, B, or C sources without the presence of a catalyst to irradiate a polluted aqueous solution, whereas a photochemical reaction is a chemical reaction induced or catalyzed by light. The primary step in UV photolysis is the electronic excitation of the substrate, S, followed by electron transfer from the excited state, S^* , to ground state molecular oxygen, O_2 :

$$S + hv \to S^* \tag{1.31}$$

$$S^* + O_2 \rightarrow S^{+} + O_2^{-}$$
 (1.32)

Through homolytic scission, free radicals form and further reaction of these species with dissolved oxygen generates peroxide radicals. The formation of reactive oxygen species and radicals leads to the degradation of the parent compound. Photolysis of $\rm H_2O_2$ and $\rm O_3$ is used in water treatment.

1.4.2.2 Ozonation Processes

Ozonation involves two species of interest: (i) ozone and (ii) hydroxyl radicals. Ozone is able to decompose into hydroxyl radicals. Disinfection occurs predominantly with ozone, which is a very selective oxidant compared to hydroxyl radicals which react nonselectively. NOM is converted into oxidized compounds and total degradation end-products through electrophilic attack or dipolar cyclo-addition [68]. Ozonation processes that are found in water treatment are O₃, UV/O₃, and O₃/H₂O.

1.4.2.3 Fenton and Photo-Fenton Processes

The reaction of ferrous iron with H_2O_2 leads to the formation of ferric iron and hydroxyl radical [69]. Dark and photo-Fenton reactions take place under acidic

 Table 1.8 Overview of AOP processes and their reaction mechanisms

AOP process	Description	Reaction mechanism
Photo-induced advanced oxidation processes	UV/H ₂ O ₂ H ₂ O ₂ is injected and mixed into the feed water and enters a reactor equipped with UV lights. The direct photolysis, at a wavelength of 254 nm, of hydrogen peroxide leads to the formation of HO' radicals UV/O ₃ Ozone adsorbs UV radiation at 330 nm or less. H ₂ O ₂ is produced as an intermediate, which later decomposes to HO'	$\begin{split} &H_2O_2 + h\nu \; (\lambda < 254 \; nm) \to 2HO^{\cdot} \\ &H_2O_2 + HO^{\cdot} \to HO_2 + H_2O \\ &H_2O_2 + HO_2 \to HO^{\cdot} + H_2O + O_2 \\ &HO_2 + HO_2 \to H_2O_2 + O_2 \end{split}$ $&O_3 + H_2O + h\nu \; (\lambda < 330 \; nm) \to H_2O_2 + O_2$ $&H_2O_2 + h\nu \to 2HO^{\cdot} \\ &O_3 + H_2O_2 \to H_2O + 2O_2 \end{split}$
	VUV Extreme UV irradiation of H ₂ O at wavelengths below 190 nm is able to lyse H ₂ O and generate HO radicals	$H_2O + h\nu \ (\lambda < 190 \text{ nm}) \rightarrow H^{\cdot} + HO^{\cdot}$
Ozonation	Ozone is unstable in an aqueous medium, decomposing spon- taneously and generating HO radicals	$O_3 + HO \rightarrow O_3 - HO$ $O_3^- \rightarrow O_2^+ + HO$ $O_3^- \rightarrow HO$
Fenton and Photo- Fenton processes	Fenton process Fenton's reagent, a mixture of ferrous iron and H ₂ O ₂ is used to catalytically decompose H ₂ O ₂ into OH'radicals. The ferrous iron catalyst is oxidized into ferric iron and reduced back to ferrous iron by the same H ₂ O ₂ source Photo-Fenton Process Exposing UV light to the Fenton reagent can also generate HO'	$\begin{split} & Fe^{2+} + H_2O_2 \rightarrow Fe^{3+} + [H_2O_2 -] \\ & + HO^{\cdot} + OH - \\ & Fe^{3+} + H_2O_2 \rightarrow Fe^{2+} + HO_2^{\cdot} - + H + \\ & Fe^{2+} + HO^{\cdot} \rightarrow Fe^{3+} + OH - \\ \end{split}$
Sensitized processes	radicals TiO ₂ semiconductor photocatalysis TiO ₂ in aqueous solution acts as a photocell in which UV light with a wavelength of less than 390 nm can generate electron and hole pairs. These electron/ hole pairs participate in redox reactions and produce HO' radicals	$H_2O_2 + O_2 \rightarrow HO^{\cdot} + O_2 + OH - H_2O_2 + TiO_2(e_{CB^-}) \rightarrow TiO_2 + HO^{\bullet} + OH^-$

(continued)

AOP process	Description	Reaction mechanism
Sonolysis	Ultrasonic irradiation generates high local temperatures and pressures as a result of acous- tic cavitation resulting in HO production	$\begin{split} R & \xrightarrow{\Delta + ultrasonic} pyrolysis \ product \\ H_2O & \xrightarrow{\Delta + ultrasonic} H^{\bullet} + HO^{\bullet} \\ HO \cdot + R & \xrightarrow{\Delta + ultrasonic} product \end{split}$

Table 1.8 (continued)

Adapted from Belgiorno et al. (2011), Ref. [9]; Gottschalk and Libra (2000), Ref. [71]

conditions, and irradiation of the Fenton process by visible or near-UV radiation considerably improves the rate of removal of pollutants.

1.4.2.4 Sensitized Processes

Sensitized AOPs can be classified as either dye-sensitized and semiconductor-sensitized processes. In a dye-sensitized process, the dye molecules absorbing visible light are excited to a higher energy state. The excited dye transfers its excess energy to other molecules in the reaction medium producing a chemical reaction. When dissolved oxygen is present, it accepts energy from the excited dye molecule and the dissolved oxygen is converted to singlet oxygen, which is a strong oxidant. Semiconductor-sensitized processes are concerned with the effect of light on interacting molecules and solid semiconductor surfaces like TiO₂. The process depends on the formation of electron—hole pairs upon irradiation of light energy exceeding the energy of the band gap of the semiconductor.

1.4.2.5 Sonolysis

Ultrasonic irradiation, or sonolysis, can be employed for the degradation of many organic compounds. Ultrasound irradiation alone has not been able to provide sufficient degradation rates; especially for hydrophilic compounds. The degradation rate by sonolysis alone is much slower than other AOPs. Ultrasound destroys organics by cavitation of small bubbles. Extremely high temperatures and pressures occur during bubble cavitation at a localized region. This causes pyrolysis of organic molecules and produces reactive chemical radicals. The estimated transient temperature is about 4,000–10,000 K and the pressure is in the range of 30–98 MPa [70]. As a result of cavitation, two processes occur that degrade organics: (i) pyrolysis due to high temperature and pressures and (ii) the production of radical species.

Table 1.9 Common AOPs and their advantages and disadvantages

AOP	Advantages	Disadvantages
H ₂ O ₂ – UV	 H₂O₂ is relatively stable and can be stored for long periods UV irradiation can serve as disinfectant Capable of full-scale drinking water treatment 	 Turbidity affects UV light penetration Special reactors for UV illumination are required Residual H₂O₂ must be addressed
O ₃	 Very strong oxidant with short reaction time Can eliminate wide variety of organic and inorganic contaminants The treatment does not add chemicals to the water 	 High capital and maintenance costs Energy intensive Potential fire hazard and toxicity pH adjustment required and not practical
O ₃ –H ₂ O ₂	 High efficiency Waters with poor UV transmission can be treated and custom reactors for UV are not required Disinfection Established technology for remediation 	 Potential for bromate formation Energy and cost-intensive May require treatment of excess H₂O₂ due to potential for microbial growth Must maintain proper O₃/H₂O₂ dosages Low pH is detrimental to the process
O ₃ –UV	 Residual oxidant will degrade rapidly Ozone adsorbs more UV light than hydrogen peroxide (more efficient that H₂O₂/UV) UV irradiation can serve as disinfectant 	 Energy and cost-intensive Custom reactors for UV irradiation are required Volatile compounds are stripped from the process Turbidity affects UV light penetration Ozone diffusion can result in mass transfer limitations Potential increase in trihalomethanes (THM) and haloaceticacids (HAA) formation when combined with chlorine disinfection
TiO ₂ – UV	Activated at near UV light (300–380 nm) compared to other UV oxidation pro- cesses that require lower wavelengths	 Fouling of catalyst may occur When used as a slurry, TiO₂ must be recovered
Sonolysis	 Useful with waters with low light penetration Economical treatment of small volumes 	 Increases water turbidity High energy consumption High maintenance costs of probes Design criteria is still being developed
Fenton	 Some groundwaters have sufficient Fe to drive Fenton's reaction Not energy intensive like O₃, UV, or sonolysis Commercial processes are available 	 Low pH (<2.5) is required so that iron does not precipitate Requires iron extraction system Operational costs associated with pH adjustment

Adapted from Belgiorno et al. (2011), Ref. [9]; Crittenden et al. (2012), Ref. [22]

1.4.2.6 Major Factors that Impact AOPs

The major factors that impact AOPs are pH, carbonate, NOM, and reduced metal ions. The performance of AOPs is affected by pH in three ways: (i) pH affects the charge on organic compounds that are slightly acidic or basic, (ii) pH affects the concentration of HCO₃⁻ and CO₃²⁻, and (iii) pH affects the concentration of HO₂⁻, which is important in UV/H₂O₂, UV/O₃, and H₂O₂/O₃ AOPs. For these AOPs, low pH (<5.0) reduces the rate of production of HO [72]. Bicarbonate and carbonate ions are HO radical scavangers and are often found in high concentrations compared to the concentration of organic pollutant [73]. NOM reacts with HO radicals and quenches the reaction [74, 75]. Metal ions in reduced oxidation states, such as Fe (I) and Mn (II), can consume a significant amount of chemical oxidants, and can scavenge HO radicals.

1.4.3 Semiconductor Photocatalytic Degradation

1.4.3.1 Semiconductor Basics

1.4.3.1.1 General Characteristics of Semiconductors

The de Broglie relation associates a wavelength with the electron as follows:

$$\lambda = \frac{h}{p} = \frac{h}{mv} \tag{1.33}$$

where h is Planck constant and p is momentum.

The wavelength is a function of the inverse of the momentum of the particle and the frequency is a function of the particle's kinetic energy:

$$f = \frac{E}{h} \tag{1.34}$$

The wave number corresponds to the number of repeating units per unit of space:

$$\overline{v} = \frac{1}{\lambda} \left(\overline{v} = \frac{f}{v} \right)$$
 for non-dispersive waves and $\overline{v} = \frac{f}{c}$ for electromagnetic waves (1.35)

where v is propagation velocity of the wave (m s⁻¹) and c is speed of light (m s⁻¹). The wave vector is a vector related to a wave, and its amplitude is equal to the wave number while its direction is that of the propagation of the wave:

$$\overline{k} = \frac{2\pi}{\lambda} \tag{1.36}$$

Therefore the electron momentum can be expressed as:

$$\overline{p} = \frac{\hbar}{\lambda} = \hbar \overline{k} \tag{1.37}$$

where $\overline{h} = \frac{h}{2\pi}$ is reduced Plank constant.

In the free electron model, the electron energy is therefore:

$$E = \frac{p^2}{2m} = \frac{\hbar^2 \overline{k}^2}{2m} \tag{1.38}$$

where m is inertial mass of the wave-particle.

As m varies with the wave vector, it is called effective mass (m^*) , defined as:

$$m^* = \frac{\hbar^2}{\partial^2 E/\partial k^2} \tag{1.39}$$

In a free electron the wave function are plane waves, defined as:

$$\Psi_k(r) = e^{ikr} \tag{1.40}$$

When an electron is placed in a periodic potential such as a crystal lattice with a lattice distance of a, the wave function of the electron is known as the Bloch wave function [76]:

$$\Psi_{nk}(r) = e^{ikr} U_{nk}(x) \tag{1.41}$$

where U(x) is a periodic function that matches the periodic potential (U(x+a) = U(x)).

In the propagation of a wave through a crystal lattice, the frequency is a periodic function of some wave vector k, in which multiple solutions to the Schrödinger equation exist, labeled by n, the band index that numbers the energy bands. Each of these energy levels, with changes in k, forms a smooth band of states. For each band, a function $E_n(k)$ can be defined. The wave vector takes on any value inside what is known as the Brillouin zone [77], which is a polyhedron in reciprocal space of the crystal lattice.

Energy band gaps can be classified as either direct or indirect band gaps (Fig. 1.5). A semiconductor is called a direct band gap semiconductor if the energy of the top valence band lies below the minimum energy of the conduction band without a change in momentum. On the other hand, a semiconductor is called an indirect band gap semiconductor if the minimum energy in the conduction band is shifted by a change in momentum Δp .

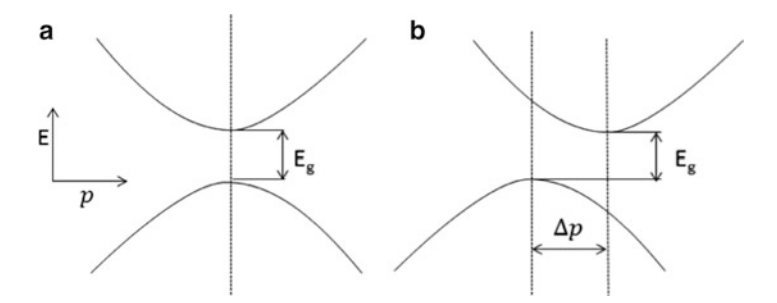


Fig. 1.5 Energy vs. Momentum diagram for a (a) direct bandgap semiconductor and (b) an indirect band gap semiconductor

The probability f(E), that an energetic level of a solid is occupied by electrons, is determined by the Fermi-Dirac distribution function [78]:

$$f(E) = \frac{1}{1 + \exp\frac{(E - E_F^o)}{k_B T}}$$
(1.42)

where *E* is energy (J), E_F^o is Fermi level (J), k_B is Boltzmann constant (1.3806 10^{-23} m² kg s⁻² K⁻¹), and *T* is temperature (K).

The Fermi level (E_F^o) represents the 50 % probability of finding an electron in this level. For intrinsic semiconductors, E_F^o falls inside the energetic gap and depends on the mass of electrons at the end of the conduction band (m_e^*) , on the effective mass of electrons at the beginning of the valence band (m_h^*) , and on the amplitude of the band gap (E_g) . The equation of the Fermi level is as follows:

$$E_F^o = \frac{1}{2} E_G + \frac{3}{4} kT \ln \left(\frac{m_h^*}{m_e^*} \right)$$
 (1.43)

The value of E_F^o is equivalent to the electrochemical potential of an electron.

1.4.3.1.2 Semiconductor Doping

Some types of impurities and imperfections to the crystal lattice may drastically affect the electrical properties of a semiconductor. The conductivity of a semiconductor can be increased by doping, a technique that introduces foreign atoms into the lattice. This makes electrons available in the conduction band and holes available in the valence band. For example, in the case of the Si lattice, with each Si atom having four covalent bonds with four nearby Si atoms, the addition of atoms—arsenic, phosphorous, or antimony—having one more valence electron

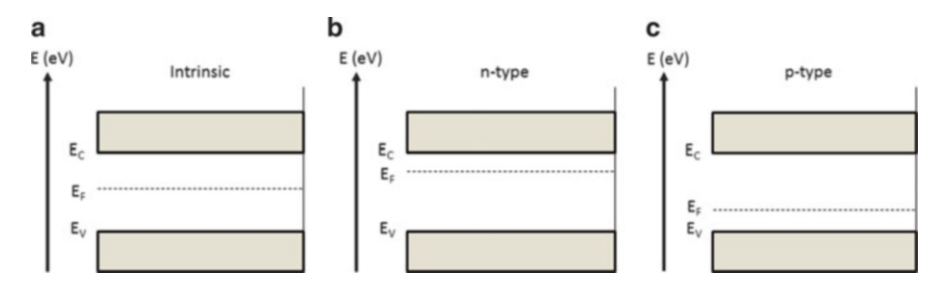


Fig. 1.6 Three types of semiconductors: (a) intrinsic, (b) n-type, and (c) p-type

compared to Si will lead to an excess positive charge due to the transfer of an electron from the foreign atom to the conduction band. This is called donor doping and creates an n-type semiconductor, where the Fermi level will be close to the conduction band. On the other hand, if the foreign atom is boron, gallium, and indium, which have one valence electron less than Si, it can accept one electron from the valence band. This is called acceptor doping and creates a p-type semiconductor, where the Fermi level will reside closer to the valence band. The Fermi levels of intrinsic, n-type, and p-type semiconductors are shown in Fig. 1.6.

1.4.3.1.3 Semiconductor in Electrolyte

The energy levels of electrons in solids can be extended to the case of an electrolytic solution containing a redox system [79]. The occupied electronic levels correspond to energetic states of reduced species, whereas unoccupied states correspond to energetic states of oxidized species. The Fermi level of the redox couple, $E_{\rm f, redox}$, corresponds to the electrochemical potential of electrons in the redox system and is equivalent of the reduction potential V_o . To correlate energetic levels of the semiconductor and the redox couple in an electrolyte, two different scales are used (in eV and V). There are two scales because in solid-state physics zero is the level of an electronic vacuum and in electrochemistry the reference is the potential of the normal hydrogen electron (NHE). The two scales are correlated using the potential of NHE, which is equal to $-4.5~{\rm eV}$ and is referred to as that of the electron in a vacuum [80].

If a semiconductor is placed in contact with a solution containing a redox couple, equilibrium is reached when the Fermi levels of both phases become equal. This occurs by means of an electron exchange from solid and electrolyte, which leads to the generation of charge inside the semiconductor. This charge is distributed in a spatial charge region near the surface, in which the value of holes and electron concentrations also differ considerably from those inside the semiconductor. Figure 1.7a shows schematically the energetic levels of an *n*-type semiconductor and a redox electrolyte before contact and at equilibrium after contract. In particular, as the energy of the Fermi level is higher than that of the electrolyte,

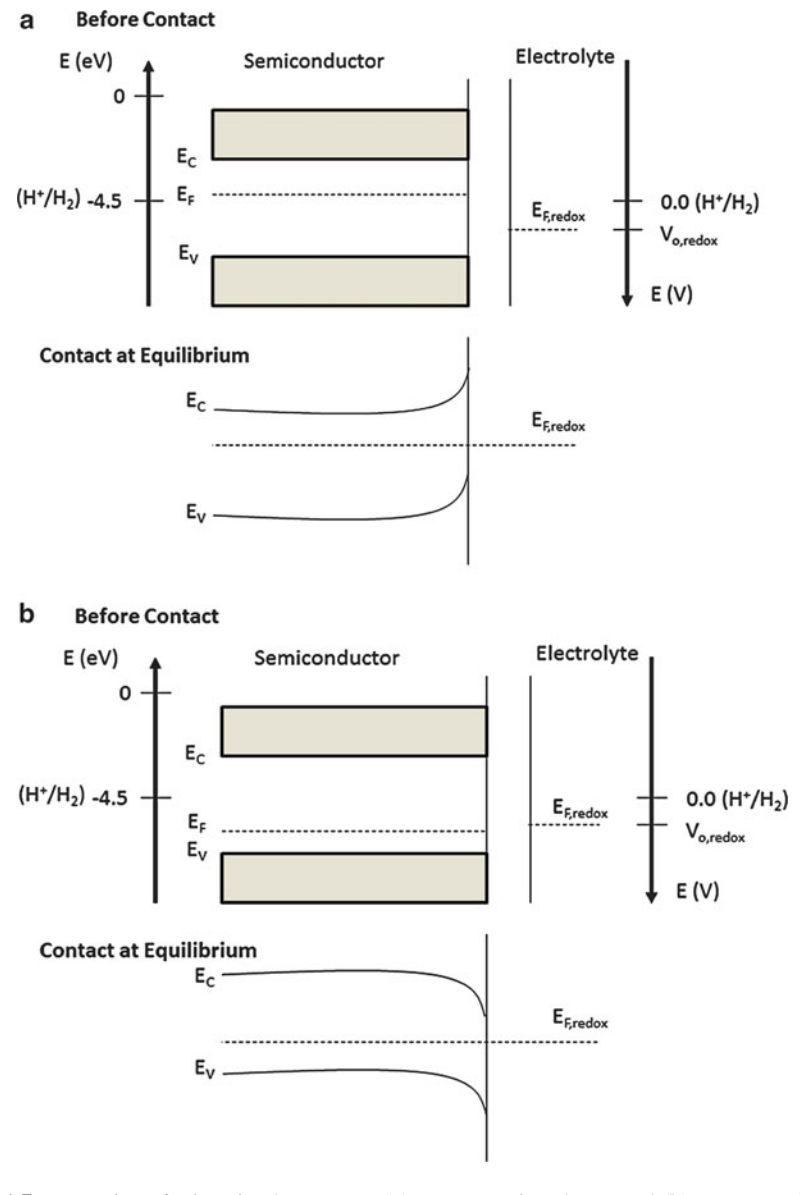


Fig. 1.7 Formation of a junction between an (a) n-type semiconductor and (b) p-type semiconductor in an electrolyte solution before contact and at equilibrium after contact

equilibrium is reached by electron transfer from the semiconductor r to the solution. An electric field is produced by this electron transfer, which is represented by upward band bending. Owing to the presence of the field, holes in excess generated in the spatial charge region move toward the semiconductor surface, whereas electrons in excess migrate from the surface to the bulk of the solid. Figure 1.7b

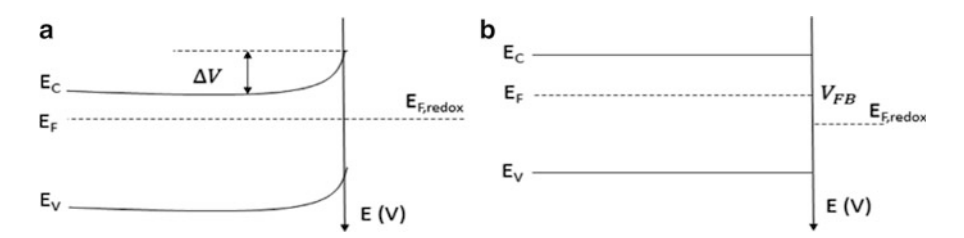


Fig. 1.8 Scheme of the energetic levels at the interface semiconductor-electrolyte for an n-type semiconductor at (a) equilibrium and (b) flat band potential

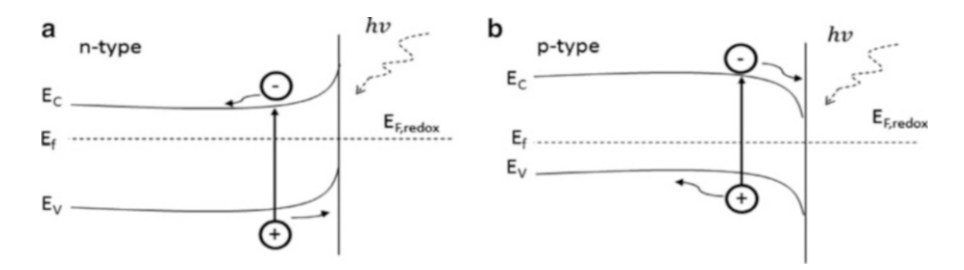


Fig. 1.9 Generation of an electron-hole pair after irradiation of (a) n-type semiconductor and (b) p-type semiconductor

shows the contact between a redox electrolyte and a p-type semiconductor. In this case transfer of electrons occurs from the electrolyte to the semiconductor and band bending is downward.

If the potential of the electrode changes due to an anodic or cathodic polarization, a shift of the Fermi level of the semiconductor with respect to that of the solution occurs with an opposite curvature of the bands as seen in Fig. 1.8. For a particular value of the electrode potential, the charge excess disappears and the bands become flat from the bulk to the surface of the semiconductor. The corresponding potential is called the flat band potential, $V_{\rm FB}$, and the determination of this potential allows for the calculation of the energy of the conduction and the valence bands [81].

When a semiconductor is irradiated by radiation of suitable energy equal to or higher than that of the band gap, E_g , electrons can be promoted from the valence band to the conduction band. Figure 1.9 shows the scheme of electron-hole pair formation due to the adsorption of a photon by a semiconductor.

The existence of an electric field in the spatial charge region allows for the separation of the photogenerated pairs. In the case of n-type semiconductor, electrons migrate toward the bulk whereas holes move to the surface. In the case of p-type semiconductors, holes move toward the bulk whereas electrons move to the surface.

Photoproduced holes and electrons, during their migration in opposite directions, can (i) recombine and dissipate their energy as either electro-magnetic

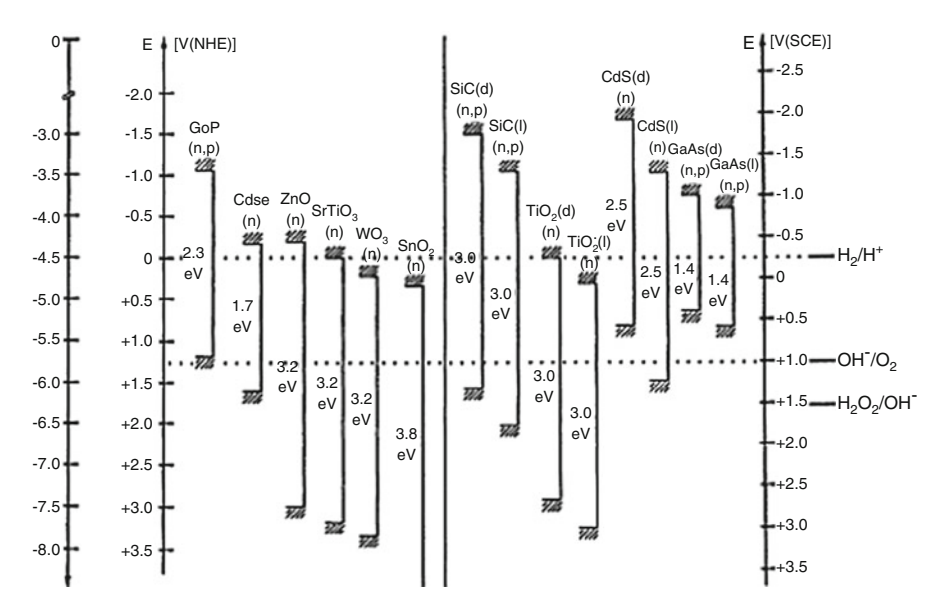


Fig. 1.10 Positions of band edges for some semiconductors in contact with aqueous electrolyte at pH 0. *Source*: Memming (1994), Ref. [82]

radiation (photon emission) or simply as heat, or (ii) react with electron-acceptor or electron-donor species present at the semiconductor electrolyte interface, thereby reducing or oxidizing them, respectively.

The energy of the conduction band edge (E_c) corresponds to the potential of the photogenerated electrons, whereas the energy of the valence band gap corresponds to the potential of the holes. If E_c is more negative than the potential of a species present in solution, electrons reaching the interface can reduce the oxidized form of the redox couple. Conversely, if the potential of E_v is more positive than that of the redox couple, photoproduced holes can oxidize its reduced form. Knowledge of the relative edge positions of the bands and of the energetic levels of the redox couples is essential to establish if thermodynamics allow the occurrence of oxidation and/or reduction of the species in solution. The band gaps and the positions of the valence band and conduction band edges for various semiconductors are given in Fig. 1.10.

1.4.3.2 Photocatalysis Mechanism

Photocatalytic properties of a semiconductor depend on (i) the position of the energetic levels; (ii) the mobility and mean lifetime of the photogenerated electrons and holes, (iii) the light absorption coefficient, and (iv) the nature of the interface. The photoactivity depends on the method of preparation of the catalyst, where the physicochemical properties of the semiconductor are altered.

Each particle of semiconductor in a photocatalytic system is akin to a photoelectrochemical cell using a semiconductor electrode in contact with an electrode of an inert metal [83]. In a photoelectrochemical cell an oxidation or reduction reaction may occur on the semiconductor electrode, whereas in a semiconductor particle immersed in an electrolyte solution both reactions occur simultaneously via hole transfer from the valence band and by electron transfer from the conduction band.

A semiconductor powder suspension is a mixture of many small photocells. Separation of electron–hole pairs increases with increasing thickness of the spatial charge region, which depends on the doping of the semiconductor. As the volume of the semiconductor particle decreases, charge separation becomes a minimum when the particle size is smaller than the thickness of the spatial charge region. The adsorption of radiation of a suitable wavelength by the semiconductor allows the transformation of photons into chemical energy; this phenomenon is termed photocatalysis. When aqueous solutions of semiconductor powders are irradiated at the solid–liquid interface of the photocatalyst, photo-induced chemical reactions occur that are able to degrade organic and inorganic molecules. Degradation occurs directly by the electron–hole pairs, or via formation of reactive radical species that are generated in the presence of O_2 and H_2O . The photocatalytic process also eliminates many inorganic ionic pollutants present in water by reduction into elemental form in the vicinity of the catalyst particle or transformation into less noxious species.

1.4.3.3 Kinetics of Photocatalysis

Heterogeneous catalysis involves systems in which reactants and catalyst are physically separated phases. Photocatalysis in particular is a change in the rate of a chemical reaction or its generation when a semiconductor, the photocatalyst, absorbs ultraviolet-visible-infrared radiation. Photocatalysis taking place at the boundaries between two phases can be expressed as:

$$A \xrightarrow{\text{hv, catalyst}} B \tag{1.44}$$

where A is reactant and B is product.

Photocatalysis of a heterogeneous system can be thought of as two steps: (i) photoadsorption/desorption processes and (ii) photoexcitation. Photosorption can be represented as:

$$A \xrightarrow{\text{hv, catalyst}} A_{\text{ads}}$$
 (1.45)

where A is reactant and A_{ads} photoadsorbed species.

The photoadsorption of oxygen is focused on TiO₂ surface [84–88]. Photoadsorbed species can act as surface-hole trappings and photoelectrons can be trapped in the bulk

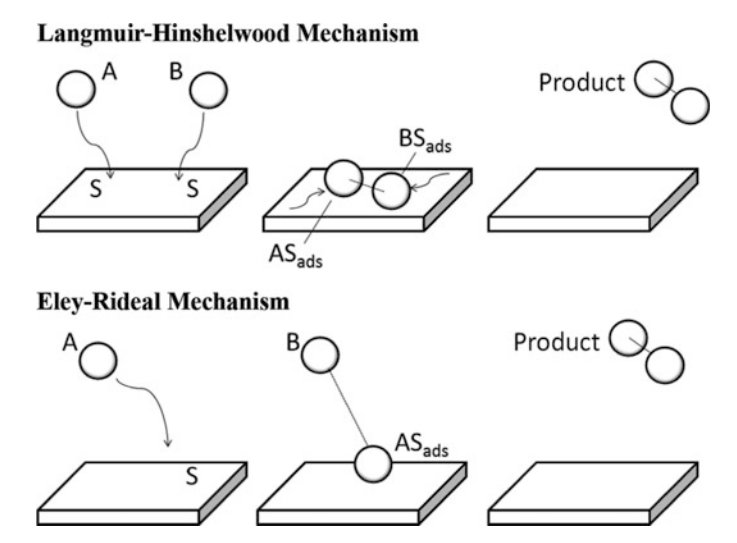


Fig. 1.11 Top model: Langmuir-Hinshelwood Mechanism—two molecules adsorb onto the surface and diffuse and interact with each other until a product is formed and desorbs from the surface; Bottom model: Eley-Rideal Mechanism—a molecule adsorbs onto the surface and another molecule interacts with the adsorbed one until a product is formed and desorbs from the surface

of the solid or as surface electron trappings. It will depend on the chemical nature of the molecule adsorbed and on the type of the solid adsorbent. These changes are generally fast and reversible, such that once irradiation has stopped the surface recovers its previous features under equal initial conditions.

Photoexcitation of a semiconductor can be separated into four simplified types of electronic excitations induced by light adsorption. In a perfect crystal lattice, absorption can produce only intrinsic photoexcitations with (i) the promotion of electrons from the valence band to the conduction band forming free electron-hole pairs and (ii) the formation of free bulk excitons (the combination of an electron and a positive hole that is free to move through a non-metallic crystal as a unit). In an imperfect lattice, the presence of defects causes extrinsic absorption of light, in particular (iii) photon absorption due to the generation of electronically excited defects and bound and /or self-trapped excitons and (iv) photon absorption due to ionization of defect transitions between localized and delocalized electron states [89, 90].

The adsorption of molecules by the semiconductor in aqueous solution can be described by two mechanisms (Fig. 1.11): (i) the Langmuir-Hinshelwood mechanism and (ii) the Eley-Rideal mechanism. The Langmuir-Hinshelwood mechanism is used to explain the interaction of surface charge carriers and excitons with adsorbed molecules that can promote surface chemical processes, whereas the Eley-Rideal mechanism is used to explain the interaction of molecules with surface active centers that can initiate surface chemical processes.

In the Eley-Rideal mechanism [91] proposed by Eley and Rideal in 1938, only one of the reactant molecules adsorbs and the other reacts without adsorbing:

$$A + S_{\text{ads}} \leftrightarrow AS_{\text{ads}} \tag{1.46}$$

$$AS_{\text{ads}} + B_{g} \leftrightarrow \text{Product}$$
 (1.47)

In the Langmuir-Hinshelwood mechanism both molecules adsorb and then undergo a bimolecular reaction:

$$A + S \leftrightarrow AS_{\text{ads}} \tag{1.48}$$

$$B + S \leftrightarrow BS_{ads}$$
 (1.49)

$$AS_{\text{ads}} + BS_{\text{ads}} \leftrightarrow \text{Product}$$
 (1.50)

The Langmuir-Hinshelwood model (LH) is widely applied to liquid and gas phase systems for the degradation of organic substrates on ${\rm TiO_2}$ surfaces in the presence of oxygen [92–95]. It explains the kinetics of reactions that occur between two adsorbed species. The two main assumptions of the LH model are (i) the adsorption equilibrium is established at all times and the reaction rate is less than the rate of adsorption or desorption and (ii) the reaction is assumed to occur between adsorbed species whose coverage, on the catalyst surface, is in equilibrium with the concentration of the species in the fluid phase, so that the rate-determining step of the photocatalytic process is a surface reaction.

The decrease of the amount of species in a liquid–solid phase photocatalytic system is the combination of photoadsorption and photoconversion processes. To describe this system, a molar balance can be applied to the species at any time [94]:

$$n_T = n_L + n_S \tag{1.51}$$

where n_T is total number of moles present in a photoreactor (mol), n_L is number of moles in the fluid phase (mol), and n_S is number of moles photoadsorbed by the solid (mol).

The molar balance can be rearranged in terms of the total concentration of the species (C_T) (mol L⁻¹), by dividing by the volume (V) of the liquid phase (L), to obtain:

$$C_T = C_L + \frac{n_S}{V} \tag{1.52}$$

where C_L is concentration in the liquid phase (mol L^{-1}).

Both substrate and oxygen must be present for the occurrence of the photoreaction, then it is assumed that the total disappearance rate of substrate per unit surface area, r_T , relies on second-order kinetics (or a first order model with respect to the substrate coverage and oxygen coverage):

$$r_T = -\frac{1}{S} \frac{dn_T}{dt} = k'' \theta_{\text{sub}} \theta_{\text{Ox}}$$
 (1.53)

$$\theta_{\text{sub}} = \frac{n_S}{WN_S^*} \tag{1.54}$$

$$\theta_{Ox} = \frac{n_{S,Ox}}{WN_{S,Ox}^o} \tag{1.55}$$

where S is catalyst surface area (mg g⁻¹), t is time (s), k'' is second order rate constant, θ_{Sub} is substrate fractional coverage of the surface, θ_{Ox} is oxygen fractional coverage of the surface, $n_{S,Ox}$ is the number of moles of oxygen photoadsorbed on the solid on the unit mass of irradiated solid (mol), N_S^* is maximum capacity of photoadsorbed moles of substrate on the unit mass of irradiated solid (mol g⁻¹), $N_{S,Ox}^*$ is maximum capacity of photoadsorbed moles of oxygen (mol g⁻¹), and W is the mass of catalyst (g).

If oxygen is continuously bubbled into the dispersion its concentration in the liquid phase does not change and it is always in excess. The θ_{Ox} term of Eq. (1.53) is then constant so we can define $k = k''\theta_{Ox}$ and Eq. (1.53) turns to a pseudo first-order rate equation:

$$r_T = -\frac{1}{S} \frac{dn_T}{dt} = -\frac{1}{S_S W} V \frac{dC_T}{dt} = k\theta_{\text{sub}}$$
 (1.56)

where S_S surface area per unit mass of catalyst and k is pseudo first-order rate constant.

The kinetic information on a photoprocess consists of knowledge of substrate concentration values in the liquid phase, C_L , as a function of irradiation time. r_T and θ_{sub} can be formally written as a function of C_L , where θ_{sub} and C_L relations can be obtained from an appropriate isotherm (See Sect. 2.6):

$$r_T = -\frac{1}{S_S W} V \frac{dC_T(C_L)}{dt} = k\theta_{\text{sub}}(C_L)$$
 (1.57)

In a batch photocatalytic experiment, the substrate concentration values measured in the liquid phase represent the substrate concentration in equilibrium with an unknown substrate concentration on the catalytic surface. This is apparent to all the measured values of substrate concentration except for the initial one. The substrate concentration measured at the start of a photodegradation experiment is a system without irradiation, where the initial substrate concentration is under dark conditions.

1.4.3.4 Photocatalytic Materials

TiO₂ is the most widely used semiconductor photocatalyst in water treatment due to its low cost, chemical stability, and abundance. Current research focuses on increasing photocatalytic reaction kinetics and photoactivity range to provide either

high performance UV-activated photocatalytic reactors or energy-efficient solar/visible light-activated photocatalytic reactors. The optimization approaches for enhancing the reaction kinetics under UV include increasing surface area [96, 97] using 1D nano morphology [98, 99], noble metal doping [100], and producing reactive crystal facets [101, 102]. Researchers have attempted to alter the photoactivity range to solar/visible light by, for example, doping via metal impurities, anions, dyes, and narrow band-gap semiconductors [96, 100].

Other than TiO_2 , WO_3 and fullerene derivatives have potential to be used in photocatalytic water treatment. WO_3 has a narrower band gap compared to TiO_2 , allowing it to be activated by visible light (<450 nm) [103]. Fullerene derivatives such as aminofullerenes [104], fullerol, and C_{60} [105] have been proposed to generate 1O_2 under visible light irradiation, despite it currently being more expensive and less available than TiO_2 .

1.4.3.5 Physical Parameters that Affect Photo-Activity

There are five physical parameters that affect photocatalytic activity: (i) mass of catalyst, (ii) wavelength, (iii) initial concentration of reactant, (iv) temperature, and (v) radiant flux. These are shown in Fig. 1.12.

1.4.3.6 Radiation Sources

The radiation source used in a photocatalytic application largely determines the performance. There are six irradiation sources that can be used: (i) arc lamps, (ii) fluorescent lamps, (iii) incandescent lamps, (iv) lasers, (v) light-emitting diodes (LEDs), and (vi) solar light. The six processes are listed in Table 1.10 below.

Arc lamps are made from neon, argon, xenon, krypton, sodium, metal halide, and mercury. For mercury lamps, there are four classifications that have been made:

- 1. Low pressure: the lamp contains Hg vapor at 0.1 Pa at 298 K (emission wavelengths: 253.7 and 184.9 nm).
- 2. Medium pressure: the lamp contains Hg vapor from 100 kPa to several hundred kPa (emission wavelengths: 313, 366, 436, 576, and 578 nm).
- 3. High pressure: the lamp contains Hg vapor greater or equal to 10 MPa (emission: continuous background from 200 to 1,000 nm with broad lines).
- 4. Hg-Xe: the lamp contains a mixture of Hg and Xe vapors at high pressure and is used to simulate solar radiation.

Fluorescent lamps are filled with gas typically containing a mixture of low-pressure mercury vapor and argon (or xenon). The inner surface of the lamp is coated with a fluorescent coating made of vary blends of metallic and rare earth phosphor salts. The UV light produced by the cathode emits light at 253.7 and 185 nm. The UV light is absorbed by the bulb's fluorescent coating, which reradiates the energy at two intense lines of 440 and 546 nm in the visible light region.

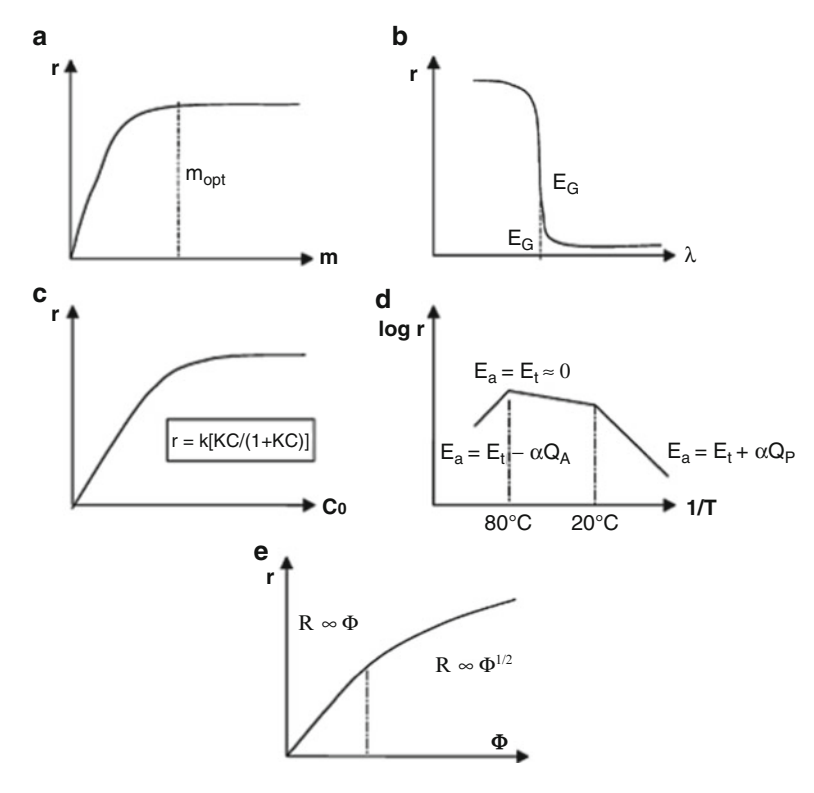


Fig. 1.12 Influence of physical parameters that affect kinetics of photocatalysis: (a) mass of catalyst; (b) wavelength λ ; (c) initial concentration of the reactant; (d) temperature; (e) radiant flux Φ . (Source: Herrmann (2010), Ref. [106]

Table 1.10 List of irradiation sources

Type of radiation source	Description of emission process
Arc lamp	Emission is obtained by activation of a gas by collision with accelerated electrons generated by an electric discharge between two electrodes, typically made from tungsten
Fluorescent lamp	The cathode is heated sufficiently to emit electrons which collide with a gas, and ionize it to form a plasma, known as impact ionization. As the conductivity of the ionized gas rises, higher currents ionize mercury causing it to emit light in the UV region of the spectrum. The UV light is adsorbed by the bulb's fluorescent coating, which re-radiates energy to lower frequencies to emit visible light.
Incandescent lamp	Emission is obtained by heating filaments of various substances to very high temperatures via current circulation
Lasers	Emission occurs via a quantum-mechanical and thermodynamic process. Light of a specific wavelength is amplified through a gain medium by a process known as pumping
Light-emitting diodes	Electrons and holes are injected in a recombination zone through two parts of the diode doped in different ways; n-type impurities for electrons and p-type for holes. When these electron-hole pairs recombined light is emitted
Solar light	Light emission from sun

An incandescent lamp is a halogen lamp, where the tungsten filament is sealed into a small envelop filled with a halogen such as iodine or bromine. In applications that required UV radiation, the lamp envelope is made of quartz and is a source of UV-B radiation. The lamp is designed to run about 2,000 h.

1.4.3.7 Quantum Yield

The quantum yield is the fundamental parameter in heterogeneous photocatalysis and is described as:

$$\Phi_{\lambda} = \frac{\text{moles of reactant or product}}{\text{moles of photons (einsteins)adsorbed}}$$
(1.58)

This parameter is useful as a way to compare efficiencies between various photocatalysts; however, there are two experimental issues: (i) most common light sources are not monochromatic and (ii) the inherent difficulty of measuring the photons adsorbed by the photocatalyst. For photocatalytic reactions in aqueous solutions, a standard protocol has been proposed that uses a standard reactant, such as phenol, and a standard photocatalyst (Degussa P25) to compare results from any laboratory or experimental arrangement in terms of quantum yield. The apparent quantum yield for most photocatalytic reaction range from 0.1 to 3 % depending on the following properties: (i) reactant and its concentration, (ii) light intensity, and (iii) the constituents in the water matrix. There are examples of increasing the quantum yield, such as by reducing catalyst electron–hole recombination. This is an area where ongoing research is being conducted [91].

References

- 1. A. Hazen, Clean Water and How to Get It (Wiley, New York, 1909)
- 2. G.W. Fuller, Progress in water purification. J. AWWA 25(11), 1566–1576 (1933)
- S. Malato, P. Fernández-Ibáñez, M.I. Maldonado, J. Blanco, W. Gernjak, Decontamination and disinfection of water by solar photocatalysis: recent overview and trends. Catal. Today 147(1), 1–59 (2009)
- S.D. Richardson, A.D. Thurston, T.W. Collette, K.S. Patterson, B.W. Lykins, J.C. Ireland, Identification of TiO2/UV disinfection byproducts in drinking water. Environ. Sci. Technol. 30, 3327–3334 (1996)
- S. Suárez, M. Carballa, F. Omil, J.M. Lema, How are pharmaceutical and personal care products (PPCPs) removed from urban wastewaters? Rev. Environ. Sci. Biotechnol. 7, 125–138 (2008)
- 6. T. Wintgens, F. Salehi, R. Hochstrat, T. Melin, Emerging contaminants and treatment options in water recycling for indirect potable use. Water Sci. Technol. **57**(1), 99–107 (2008)
- L. Bousselmi, S.U. Geissen, H. Schroeder, Textile wastewater treatment and reuse by solar catalysis: results from a pilot plant in Tunisia. Water Sci. Technol. 49(4), 331–337 (2004)

- 8. S. Mozia, M. Tomaszewska, A.W. Morawski, Photocatalytic membrane reactor (PMR) coupling photocatalysis and membrane distillation—effectiveness of removal of three azo dyes from water. Catal. Today **129**(1–2), 3–8 (2007)
- V. Belgiorno, V. Naddeo, L. Rizzo, Water, Wastewater and Soil Treatment by Advance Oxidation Processes (Lulu, Raleigh, NC, 2011)
- L. Rizzo, S. Meric, M. Guida, D. Kassinos, V. Belgiorno, Heterogeneous photocatalytic degradation kinetics and detoxification of an urban wastewater treatment plant effluent contaminated with pharmaceuticals. Water Res. 43(16), 4070–4078 (2009)
- S.A. Snyder, P. Westerhoff, Y. Yoon, D.L. Sedlak, Pharmaceuticals, personal care products, and endocrine disruptors in water: implications for the water industry. Environ. Eng. Sci. 20(5), 449–469 (2003)
- 12. J. Theron, J.A. Walker, T.E. Cloete, Nanotechnology and water treatment: applications and emerging opportunities. Crit. Rev. Microbiol. **34**(1), 43–69 (2008)
- 13. J.W. Hassler, Activated Carbon (Chemical Publishing, New York, 1974)
- M.N. Baker, The Quest for Pure Water, vol. 1, 2nd edn. (American Water Works Association, Denver, CO, 1981)
- 15. H. Sontheimer, J.C. Critenden, R.S. Summers, *Activated Carbon for Water Treatment*, 2nd edn. (DVGW-Forschumgsstelle, University of Karlsruhe, Germany, 1988). Distributed in the US by the American Water Works Association
- R.S. Summers, D.R.U. Knappe, V.L. Snoeyink, Adsorption of organic compounds by activated carbon, in *Water Quality and Treatment*, ed. by J.K. Edzwald, 5th edn. (McGraw-Hill and American Water Works Association, New York, 2010)
- Z.K. Chowdhury, R.S. Summers, G.P. Westerhoff, B.J. Leto, K.O. Nowack, C.J. Corwin, L.B. Passantino, *Activated Carbon: Solutions for Improving Water Quality* (American Water Works Association, Denver, CO, 2013)
- 18. G. Nemethy, H.A. Scherage, Structure of water and hydrophobic bonding in proteins. I. A model for the thermodynamic properties of liquid water. J. Chem. Phys. 36, 3382–3401 (1962)
- 19. M. Terrones, Science and technology of the twenty-first century: synthesis, properties and applications of carbon nanotubes. Ann. Rev. Mater. Res. 33, 419–501 (2003)
- C. Kemp, H. Seema, M. Saleh, H. Le, K. Mahesh, V. Chandra, K.S. Kim, Environmental applications using grapheme composites: water remediation and gas adsorption. Nanoscale 5, 3149–3171 (2013)
- T.T. Teng, L.W. Low, Removal of dyes and pigments from industrial effluents, in *Advances in Water Treatment and Pollution Prevention*, ed. by S.K. Sharma, R. Sanghi (Springer, The Netherlands. 2012)
- J.C. Crittenden, R.R. Trussel, D.W. Hand, K.J. Howe, G. Tchobanoglous, MWH's Water Treatment—Principles and Design, 3rd edn. (John Wiley & Sons, 2012)
- G. Crini, Non-conventional low-cost adsorbents for dye removal: a review. Bioresour. Technol. 97, 1061–1085 (2006)
- 24. G. McKay, J.F. Porter, G.R. Prasad, The removal of dye colours from aqueous solutions by adsorption on low-cost materials. Water Air Soil Pollut. **114**, 423–438 (1999)
- B.H. Hameed, Evaluation of papaya seeds as a novel non-conventional low-cost adsorbent for removal of methylene blue. J. Hazard. Mater. 162, 939–944 (2009)
- Y.H. Magdy, A.A.M. Daifullah, Adsorption of a basic dye from aqueous solutions onto sugar-industry-mud. Waste Manag. 18, 219–226 (1998)
- 27. B.H. Hameed, Grass waste: a novel sorbent for the removal of basic dye form aqueous solution. J. Hazard. Mater. **166**, 233–238 (2009)
- 28. B.H. Hameed, D.K. Mahmoud, A.L. Ahmad, Sorption of basic dye from aqueous solution by pomelo (Citrus grandis) peel in a batch system. Colloids Surf. A **316**, 78–84 (2008)
- B.H. Hameed, A.A. Ahmad, Batch adsorption of methylene blue from aqueous solution by garlic peel, an agricultural waste biomass. J. Hazard. Mater. 164, 870–875 (2009)
- N.A. Oladoja, I.O. Asia, C.O. Aboluwoye, Y.B. Oladimeji, A.O. Ashogbon, Studies on the sorption of basic dye by rubber (Hevea brasiliensis) seed shell. Turk. J. Eng. Environ. Sci. 32, 143–152 (2008)

31. D.S. Sun, X.D. Zhang, Y.D. Wu, X. Liu, Adsorption of anionic dyes from aqueous solution on fly ash. J. Hazard. Mater. **181**, 335–342 (2010)

- 32. T.C. Hsu, Adsorption of an acid dye onto coal fly ash. Fuel 87, 3040-3045 (2008)
- S. Senthilkumaar, P. Kalaamani, K. Porkodi, P.R. Varadarajan, C.V. Subburaam, Adsorption
 of dissolved reactivered dye from aqueous phase onto activated carbon prepared from
 agricultural waste. Bio. Resour. Technol. 97, 1618–1625 (2006)
- C.A.P. Almeida, N.A. Debacher, A.J. Downs, L. Cottet, C.A.D. Mello, Removal of methylene blue from colored effluents by adsorption on momtmorillonite clay. J. Colloid Interface Sci. 332, 46–53 (2009)
- 35. S. Hong, C. Wen, J. He, F. Gan, Y.S. Ho, Adsorption thermodynamics of methylene blue onto bentonite. J. Hazard. Mater. **167**, 630–633 (2009)
- 36. M. Hajjaji, A. Alami, A. El-Bouadili, Removal of methylene blue from aqueous solution by fibrous clay minerals. J. Hazard. Mater. 135, 188–192 (2006)
- 37. A. Al-Futaisi, A. Jamrah, R. Al-Hanai, Aspects of cationic dye molecule adsorption to palygorskite. Desalination **214**, 327–342 (2007)
- 38. S. Chakrabarti, B.K. Dutta, Note on the adsorption and diffusion of methylene blue in glass fibers. J. Colloid Interface Sci. **286**, 807–811 (2005)
- 39. V. Vimonses, S.M. Lei, B. Jin, C.W.K. Chow, C. Saint, Adsorption of Congo red by three Australian kaolins. Appl. Clay. Sci. 43, 465–472 (2009)
- 40. K. Marungrueng, P. Pavasant, High performance biosorbent (Caulerpa lentillifera) for basic dye removal. Bioresour. Technol. 98, 1567–1572 (2007)
- 41. O. Gulnaz, A. Kaya, F. Matyar, B. Arikan, Sorption of basic dyes from aqueous solution by activated sludge. J. Hazard. Mater. 108, 183–188 (2004)
- 42. E. Rubin, P. Rodriguez, R. Herrero, J. Cremades, I. Barbara, M.E. Sastre de Vicente, Removal of methylene blue from aqueous solutions using as biosorbent Sargassum muticum: an invasive macroalga in Europe. J. Chem. Technol. Biotechnol. 80, 291–298 (2005)
- 43. A. El-Sikaily, A. Khaled, A. El-Nemr, O. Abdelwahab, Removal of methylene blue from aqueous solution by marine green alga Ulva lactuca. Chem. Ecol. 22, 149–157 (2006)
- 44. D. Caparkaya, L. Cavas, Biosorption of methylene blue by a brown alga Cystoseira barbatula Kutzing. Acta. Chim. Solv. **55**, 547–553 (2008)
- M.C. Ncibi, A.M.D. Hamissa, A. Fathallah, M.H. Kortas, T. Baklouti, B. Mahjoub, M. Seffen, Biosorptive uptake of methylene blue using Mediterranean green alga Enteromorpha spp. J. Hazard. Mater. 170, 1050–1055 (2009)
- 46. T. Akar, A.S. Ozcan, S. Tunali, A. Ozcan, Biosorption of a textile dye (Acid Blue 40) by cone biomass of Thuja orientalis: estimation of equilibrium, thermodynamic and kinetic parameters. Bioresour. Technol. 99, 3057–3065 (2008)
- 47. N.S. Maurya, A.K. Mittal, P. Cornel, E. Rother, Biosorption of dyes using dead macro fungi: effect of dye structure, ionic strength and pH. Bioresour. Technol. **97**, 512–521 (2006)
- 48. K. Kumari, T.E. Abraham, Biosorption on anionic textile dyes by nonviable biomass of fungi and yeast. Bioresour. Technol. **98**, 1704–1710 (2007)
- M.P. Elizalde-González, L.E. Fuentes-Ramírez, M.R.G. Guevara-Villa, Degradation of immobilized azo dyes by Klebsiella sp. UAP-b5 isolated from maize bioadsorbent. J. Hazard. Mater. 161, 769–774 (2009)
- 50. I. Langmuir, The adsorption of gases on plane surfaces of glass, mica, and platinum. J. Am. Chem. Soc. **40**, 1361–1402 (1918)
- 51. S. Brunauer, P.H. Emmett, E. Teller, Adsorption of gases in multimolecular layers. J. Am. Chem. Soc. 60, 309–319 (1938)
- 52. H. Freundlich, *Groundwater Pollution* (Elsevier Scientific, Amsterdam, 1975)
- 53. G.D. Halsey, H.S. Taylor, Adsorption of hydrogen on tungsten powders. J. Chem. Phys. 15, 624–630 (1947)
- 54. O. Redlich, O. Peterson, A useful adsorption isotherm. J. Phys. Chem. **63**, 1024 (1959)
- 55. M.R. Wiesner, S. Chellam, Mass transport considerations for pressure-driven membrane processes. J. AWWA **84**(1), 88–95 (1992)

- K. Li, Ceramic Membranes for Separation and Reaction (Wiley, West Sussex, England, 2007)
- 57. M. Mulder, Basic Principles of Membrane Technology (Kluwer, The Netherlands, 1996)
- 58. K.J. Laidler, J.H. Meiser, *Physical Chemistry* (Houghton Mifflin, Boston, MA, 1999)
- H.F. Ridgway, H.F. Flemming, Membrane biofouling, in Water Treatment Membrane Processes, ed. by J. Mallevialle, P.E. Odendaal, M.R. Wiesner (McGraw-Hill, New York, 1996)
- G. Crozes, C. Anselme, J. Mallevialle, Effect of adsorption of organic matter on fouling of ultra filtration membranes. J. Memb. Sci. 84(1–2), 61–77 (1993)
- V. Lahoussine-Turcaud, M.R. Wiesner, J.Y. Bottero, Fouling in tangential-flow ultra filtration: the effect of colloid size and coagulation pretreatment. J. Memb. Sci. 52(2), 173–190 (1990)
- 62. C.F. Lin, T.Y. Lin, O.J. Hao, Effects of humic substance characteristics on UF performance. Water Res. **34**(4), 1097–1106 (2000)
- T. Carroll, S. King, S.R. Gray, B.A. Bolto, N.A. Booker, Fouling of microfiltration membranes by NOM after coagulation treatment. Water Res. 34(11), 2861–2868 (2000)
- 64. K.J. Howe, Effect of Coagulation Pretreatment on Membrane Filtration Performance, Ph.D. Thesis (University of Illonois at Urbana-Champaign, Urbana, IL, 2001)
- 65. W. Stumm, J.J. Morgan, Aquatic Chemistry: Chemical Equilibria and Rates in Natural Waters, 3rd edn. (Wiley, New York, 1996)
- 66. J.J. Pignatello, E. Oliveros, A. Mackay, Advanced oxidation processes for organic contaminant destruction based on the Fenton reaction and related chemistry. Crit. Rev. Environ. Sci. Technol. 36(1), 1–84 (2006)
- 67. Solarchem Environmental Systems, *The UV/ Oxidation Handbook* (Solarchem Environmental Systems, Markham, ON, 1994)
- 68. F.J. Beltran, Ozone Reaction Kinetics for Water and Wastewater Systems (Lewis, Boca Raton, FL, 2004)
- H.J.H. Fenton, Oxidation of tartaric acid in the presence of iron. Chem. Soc. H. Lond. 65, 899–910 (1894)
- M.R. Hoffmann, I. Hua, R. Höchemer, Application of ultrasonic irradiation for degradation of chemical contaminants. Water. Ultrason. Sonochem. 3, S163–S172 (1996)
- C. Gottschalk, J.A. Libra, A. Saupe, Ozonation of Water and Waste Water (Wiley-VCH, New York, 2000)
- 72. J. Hoigné, H. Bader, The role of hydroxyl radical reactions in ozonation process in aqueous solutions. Water Res. **10**(5), 377–386 (1976)
- 73. W.H. Glaze, J. Kang, Advanced oxidation processes for treating groundwater contaminated with TCE and PCE: laboratory studies. J. AWWA **81**(5), 57–63 (1988)
- 74. P. Westerhoff, G. Aiken, G. Amy, J. Debroux, Relationships between the structure of natural organic matter and its reactivity towards molecular ozone and hydroxyl radicals. Water Res. **33**(10), 2265–2276 (1999)
- P. Westerhoff, S.P. Mazyk, W.J. Cooper, D. Minakata, Electron pulse radiolysis determination of hydroxyl radical rate constants with Suwannee river fulvic acid and other dissolved organic matter isolates. Environ. Sci. Technol. 41, 4640–4646 (2007)
- F. Bloch, Über die Quantenmechanik der Elektronen in Kristallgittern. Z. Physik 52, 555–600 (1929)
- L. Brillouin, Les électrons dans les métaux et le classement des ondes de de Broglie correspondantes. C. R. Hebd. Seances Acad. Sci. 191, 292 (1930)
- 78. A.J. Dekker, Solid State Physics (Prentice-Hall, Englewood Cliffs, NJ, 1957)
- 79. H. Gerischer, An advanced treatise, in *Physical Chemistry*, vol. IX, ed. by H. Eyring, D. Henderson, W. Host (Academic Press, New York, 1970)
- F. Lohmann, Fermi-Niveau und flachbandpotential von molekülkristallen aromatischer kohlenwasserstoffe. Z. Naturforsch. Teil. A 22, 843–844 (1967)
- 81. Y.V. Pleskov, Y.Y. Gurevich, Semiconductor Photoelectrochemistry (Consultants Bureau, New York, 1986)

82. R. Memming, Photoinduced charge transfer processes at semiconductor electrodes and particles. Top. Curr. Chem. **169**, 105–181 (1994)

- 83. A.J. Bard, Photoelectrochemistry and heterogeneous photo-catalysis at semiconductors. J. Photochem. **10**, 59–75 (1979)
- 84. P. Meriaudeau, J.C. Vedrine, Electron paramagnetic resonance investigation of oxygen photoadsorption and its reactivity with carbon monoxide on titanium dioxide: the O3-3 species. J. Chem. Soc. Faraday Trans. **72**, 472–480 (1976)
- 85. W.R. Murphy, T.H. Veerkamp, T.W. Leland, Effect of ultraviolet radiation on zinc oxide catalysts. J. Catal. **43**, 304–321 (1976)
- 86. N. Sakai, R. Wang, A. Fujishima, T. Watanabe, K. Hashimoto, Effect of ultrasonic treatment on highly hydrophilic TiO₂ surfaces. Langmuir **14**, 5918–5920 (1998)
- 87. R. Wang, N. Wakai, A. Fujishima, T. Watanabe, K. Hashimoto, Studies of surface wettability conversion on TiO₂ single-crystal surfaces. J. Phys. Chem. B **103**, 2188–2194 (1999)
- 88. W.C. Wu, L.F. Liao, J.S. Shiu, J.L. Lin, FTIR study of interactions of ethyl iodide with powdered TiO₂. Phys. Chem. Chem. Phys. **2**, 4441–4446 (2000)
- A. Emeline, A. Salinaro, V.K. Ryabchuk, N. Serpone, Photoinduced processes in heterogeneous nanosystems. From photoexcitation to interfacial chemical transformations. Int. J. Photoenergy 3, 1–16 (2001)
- 90. V. Ryabchuk, Photophysical processes related to photoadsorption and photocatalysis on wide band gap solids: a review. Int. J. Photoenergy **6**, 95–113 (2004)
- 91. V. Augugliaro, L. Vittorio, M. Pagliaro, G. Palmisano, L. Palmisano, Clean by Light Irradiation: Practical Applications of Supported TiO₂ (RSC Publishing, Cambridge, UK, 2010)
- G. Palmisano, V. Loddo, S. Yurdakal, V. Auguliaro, L. Palmisano, Reaction pathways and kinetics of photocatalytic oxidation of nitrobenzene and phenylamine in aqueous TiO₂ suspensions. AIChE J. 53, 961–968 (2007)
- A. Gora, B. Toepfer, V. Puddu, G. Li Puma, Photocatalytic oxidation of herbicides in singlecomponent and multicomponent systems: reaction kinetics analysis. Appl. Catal. B 65, 1–10 (2006)
- 94. H. De Lasa, B. Serrano, M. Salaices, *Photocatalytic Reaction Engineering* (Springer, New York, 2005)
- 95. H. Ibrahim, H. De Lasa, Kinetic modeling of the photocatalytic degradation of air-bourne pollutants. AIChE J. **50**, 1017–1027 (2004)
- 96. A. Fujishima, X.T. Zhang, D.A. Tryk, TiO(2) photocatalysis and related surface phenomena. Surf. Sci. Rep. **63**(12), 515–582 (2008)
- 97. Z.B. Zhang, C.C. Wang, R. Zakaria, J.Y. Ying, Role of particle size in nanocrystalline TiO₂-based photocatalysts. J. Phys. Chem. B **102**(52), 10871–10878 (2012)
- 98. J.M. Macak, M. Zlamal, J. Krysa, P. Schmuki, Self-organized TiO₂ nanotube layers as highly efficient photocatalysts. Small **3**(2), 300–304 (2007)
- A. Hu, R. Liang, X. Zhang, S. Kurdi, D. Luong, H. Huang, P. Peng, E. Marzbanrad, K.D. Oakes, Y. Zhou, M.R. Servos, Enhanced photocatalytic degradation of dyes by TiO2 nanobelts with hierarchical structures. J. Photochem. Photobiol. A: Chem. 256(15), 7–15 (2013)
- 100. M. Ni, M.K.H. Leung, D.Y.C. Leung, K. Sumathy, A review and recent developments in photocatalytic water-splitting using TiO₂ for hydrogen production. Renew. Sust. Energ. Rev. 11(3), 401–425 (2007)
- 101. N. Murakami, Y. Kurihara, T. Tsubota, T. Ohno, Shape-controlled anatase titanium (IV) oxide particles prepared by hydrothermal treatment of peroxo titanic acid in the presence of polyvinyl alcohol. J. Phys. Chem. C 113(8), 3062–3069 (2009)
- 102. X.G. Han, Q. Kuang, M.S. Jin, Z.X. Xie, L.S. Zheng, Synthesis of titania nanosheets with a high percentage of exposed (001) facets and related photocatalytic properties. J. Am. Chem. Soc. 131(9), 3152 (2009)

- 103. H. Kominami, K. Yabutani, T. Yamamoto, Y. Kara, B. Ohtani, Synthesis of highly active tungsten(VI) oxide photocatalysts for oxygen evolution by hydrothermal treatment of aqueous tungstic acid solutions. J. Mater. Chem. 11(12), 3222–3227 (2001)
- 104. R. Lof, M. Van Veenendaal, H. Jonkman, G. Sawatzky, Band gap, excitons and Coulomb interactions of solid C 60. J. Electron Spectrosc. Related Phenomena 72, 83–87 (1995)
- 105. L. Brunet, D.Y. Lyon, E.M. Hotze, P.J.J. Alvarez, M.R. Wiesner, Comparative photoactivity and antibacterial properties of C-60 fullerenes and titanium dioxide nanoparticles. Environ. Sci. Tech. 43, 4355–4360 (2009)
- 106. J.M. Herrmann, Photocatalysis fundamentals revisited to avoid several misconceptions. App. Catal. B: Environ. **99**, 461–469 (2010)